THE ASTROPHYSICAL JOURNAL, 580:1100–1117, 2002 December 1

MODELS OF METAL-POOR STARS WITH GRAVITATIONAL SETTLING AND RADIATIVE ACCELERATIONS. III. METALLICITY DEPENDENCE

O. RICHARD,[1] G. MICHAUD,[1] AND J. RICHER[1]
Département de Physique, Université de Montréal, Montréal, PQ H3C 3J7, Canada; richard@cerca.umontreal.ca, michaudg@cerca.umontreal.ca, jacques.richer@umontreal.ca
Received 2002 May 24; accepted 2002 July 26

ABSTRACT

Evolutionary models have been calculated for Population II stars of 0.5–1.2 $M_\odot$ from the pre–main sequence to the lower part of the giant branch. Models were calculated for $Z = 0.017 \times 10^{-4}$ to 0.0068 ([Fe/H] $= -4.31$ to -0.71) to determine the effect of metallicity on the size of abundance anomalies to be expected from gravitational settling, thermal diffusion, and radiative accelerations. Rosseland opacities and radiative accelerations were calculated taking into account the concentration variations of 28 chemical species, including all species contributing to Rosseland opacities in the OPAL tables. It is shown that while radiative accelerations and gravitational settling may lead to abundance anomalies by factors of 2–10 in turnoff stars of metal-poor clusters such as M92, much smaller abundance anomalies are expected in relatively metal-rich globular clusters such as M5, M71, or 47 Tuc. Even in NGC 6397, which is only a factor of 2 more metal-rich than M92, atomic diffusion is expected to lead to smaller anomalies than in M92. In field stars with $T_{\rm eff} \geq 6000$ K and [Fe/H] < -2.3, the abundance anomalies might be even larger than in M92. Reduction of metallicity beyond [Fe/H] $= -3.31$ is shown not to cause further structural changes to models. Below that metallicity, all metals may be treated as trace elements. Comparisons are made to abundance observations in a number of clusters to determine if hydrodynamic processes competing with atomic diffusion are required by observations. For most metals the situation remains ambiguous: observations, taking into account the error bars, do not yet require additional processes. Monte Carlo simulations are used to show that the Spite plateau for Li in low-metallicity field stars remains the strongest argument for the presence of a process competing with atomic diffusion.

Subject headings: convection — diffusion — stars: abundances — stars: evolution — stars: interiors — stars: Population II — turbulence

On-line material: color figures

1. ASTROPHYSICAL CONTEXT

Gravitational settling, reinforced by thermal diffusion, has been shown by helioseismology to play an important role in the Sun (Guzik & Cox 1992, 1993; Christensen-Dalsgaard, Proffitt, & Thompson 1993; Proffitt 1994; Bahcall, Pinsonneault, & Wasserburg 1995; Guenther, Kim, & Demarque 1996; Richard et al. 1996; Brun, Turck-Chièze, & Zahn 1999). The outward flux of photons, however, leads to differential radiative pressure that must be included in stellar evolution calculations (Michaud 1970; Richer et al. 1998). In solar mass stars with solar metallicity, Turcotte et al. (1998b) have shown that while $g_{\rm rad}$ became equal to gravity for a few species around the end of the main sequence, it was never large enough to lead to observable overabundances. In low-metallicity clusters such as M92, however, it has been shown (Richard et al. 2002, hereafter Paper I) that $g_{\rm rad}$ could lead to overabundances of metals, including Fe, at the surface of turnoff stars that have masses of 0.76–0.8 $M_\odot$. A metallicity dependence of the effects of atomic diffusion is then suggested by theoretical considerations.

Observationally, some M92 stars past turnoff show star-to-star abundance variations of Li (Boesgaard et al. 1998), as well as of Fe, Mg, Na, and other species (King et al. 1998). While factor of 2 differences between Fe abundances in red giants and subgiants have been reported in M92 (King et al. 1998), Ramirez et al. (2001) and Gratton et al. (2001) find no difference between the Fe abundances in red giants and turnoff stars in clusters that have a larger Z than M92. Thévenin et al. (2001) find the same relative abundances as in the Sun in the turnoff stars of NGC 6397 with very little dispersion from star to star. A metallicity dependence of abundance anomalies in turnoff stars might then already have been observed in globular clusters. Caution is appropriate, however, since the M92 observations have larger uncertainties than those in clusters where no variation was measured.

Field stars allow the study of objects that have smaller metallicity than any cluster known. The star CD $-38°245$ has a [Fe/H] $= -3.98$ (Norris, Ryan, & Beers 2001). Norris, Beers, & Ryan (2000), for instance, argue that such stars can be used to constrain big bang nucleosynthesis, the nature of the first supernovae, the manner in which the ejecta from the first generations were incorporated into subsequent ones, and the age of the Galaxy. In other halo stars, correlations have been observed and used to rewrite the nucleosynthetic history of the low-metallicity era (Jehin et al. 1999; Thoul et al. 2002). A link with metal abundances in Lyα systems has also been suggested (Qian, Sargent, & Wasserburg 2002). A large variation in the abundance of many metals at a given [Fe/H] has been observed in very metal-deficient stars; it has been suggested that it implies variations in original relative abundances (Carretta et al. 2002). However, such interpretations assume that stars have the same surface abundances as they formed with. How are they modified if

[1] Centre de Recherche en Calcul Appliqué (CERCA), 5160 Boulevard Décarie, Bureau 400, Montréal, PQ H3X 2H9, Canada.

the abundances have changed because of transport processes? Is there a $T_{\rm eff}$ range where atomic diffusion processes have a negligible effect so that those stars may be more safely used to put constraints on nucleosynthesis? How does this $T_{\rm eff}$ interval depend on metallicity?

Ryan et al. (2001a) have observed Li deficiencies in stars whose $T_{\rm eff}$ is close to that of the hottest of the halo field stars. Some of the objects of their sample have surprisingly high $T_{\rm eff}$ for their [Fe/H], which led to the suggestion that they are blue stragglers since their $T_{\rm eff}$ is larger than seen in galactic clusters of similar [Fe/H]. Li deficiencies were also found in stars with $-2 \leq [{\rm Fe/H}] \leq -1$ by Ryan et al. (2001b), in whose sample up to 20% of stars are ultra–Li-deficient (Ryan et al. 2001a) although these authors estimate it at 7% in the whole halo population. However, is the [Fe/H] observed in those objects the original one, or could it have been modified by diffusion processes in the presence of $g_{\rm rad}$?

Salaris & Weiss (2001) questioned whether the conclusion that the Spite plateau (Spite & Spite 1982) was incompatible with models involving atomic diffusion (Michaud, Fontaine, & Beaudet 1984) was premature. They simulated the Spite plateau, taking into account the finite size of the sample, uncertainties in $T_{\rm eff}$, and a range in halo star ages. They compared their simulations to observed distributions and concluded that the statistics were not good enough to rule out evolutionary models that include atomic diffusion. How are such simulations modified if one takes into account the variation of surface [Fe/H] during evolution as well as use some of the more recent observations such as Ryan, Norris, & Beers (1999)?

Turbulent diffusion has been suggested by a number of authors as affecting the surface Li abundance in halo stars either by leading to its destruction by nuclear reactions (Pinsonneault et al. 1999; Pinsonneault, Deliyannis, & Demarque 1992; Charbonnel, Vauclair, & Zahn 1992) or by reducing the effects of atomic diffusion (Proffitt & Michaud 1991; Paper I; Théado & Vauclair 2001). We do not wish to exclude that such processes play a role in Population II stars. Neither do we wish to exclude mass loss (Vauclair & Charbonnel 1995). However, in this paper, we limit ourselves to processes that can currently be defined from first principles and compare the results to observations in order to determine when additional hydrodynamic processes are needed. We only mention turbulence again in § 7.1.

After a very brief description of the calculations (§ 2), we describe how the Population II models of various metallicities differ insofar as particle transport is concerned (§ 3). The surface abundance anomalies caused by diffusion are then shown to depend strongly on metallicity (§ 4) before they are compared to observed abundances in globular clusters (§ 5). Gratton et al. (2001) compare the Fe abundance in turnoff stars to that in subgiants, but it is important to determine if those subgiants have mixed deep enough to return to the original Fe abundances. At what $T_{\rm eff}$ and $\log g$ do abundance anomalies disappear as stars move to the giant branch? A simulation of the Li abundance to be expected in field halo stars is then attempted (§ 6) before the concluding remarks (§ 7).

2. CALCULATIONS

The models were calculated as described in Turcotte et al. (1998b) and Richard, Michaud, & Richer (2001). The radiative accelerations are from Richer et al. (1998) with the correction for redistribution from Gonzalez et al. (1995) and LeBlanc, Michaud, & Richer (2000). The atomic diffusion coefficients were taken from Paquette et al. (1986; see also Michaud & Proffitt 1993).

Models were assumed chemically homogeneous on the pre–main sequence with the abundance mix appropriate for Population II stars. The relative concentrations are defined in Table 1 of Paper I. Those of the α elements are increased compared to the solar mix ($[\alpha/{\rm Fe}] = 0.3$), as is believed to be appropriate in Population II stars (VandenBerg et al. 2000). In all models we always used the same initial mass fraction concentrations for ^{6}Li, ^{7}Li, ^{9}Be, ^{10}B, and ^{11}B (which were, respectively, 10^{-10}, 10^{-9}, 10^{-11}, 10^{-11}, and 10^{-10}).

In Turcotte et al. (1998b), the solar luminosity and radius at the solar age were used to determine the value of $\alpha_{\rm MLT}$, the ratio of the mixing length to pressure scale height, and the value of the He concentration in the zero-age Sun. The He concentration mainly affects the luminosity, while $\alpha_{\rm MLT}$ mainly determines the radius, through the depth of the surface convection zone. The required value of $\alpha_{\rm MLT}$ was found to be slightly larger in the diffusive than in the nondiffusive models because an increased value of $\alpha_{\rm MLT}$ is needed to compensate for He and metals settling from the surface convection zone. The increased $\alpha_{\rm MLT}$ in the solar models that include diffusion is then determined by the settling occurring immediately below the solar surface convection zone. See Freytag & Salaris (1999) for a discussion of uncertainties related to the use of the mixing length in Population II stars.

In one solar model with diffusion, Turcotte et al. (1998b) have calibrated $\alpha_{\rm MLT}$ using the Sun and Eddington's $T(\tau)$ relation. This is the value used here. It was also used in Paper I and in Turcotte, Richer, & Michaud (1998a). Complete series of models were calculated for $[{\rm Fe/H}] = -3.31$, -2.31, -2.01, -1.61, -1.31, and -0.71. A few models were also calculated for $[{\rm Fe/H}] = -4.31$ in order to confirm that further reduction of metallicity, below $[{\rm Fe/H}] = -3.31$, did not affect the structure of the models. The calculated series of models are identified in Table 1.

3. EVOLUTIONARY MODELS

3.1. *Convection Zones*

In Figure 1 are shown Hertzsprung-Russell diagrams, and time evolutions of $T_{\rm eff}$, temperature at the base of the surface convection zone, $T_{\rm bcz}$, and mass above the base of the surface convection zone, $M_{\rm bcz}$, of stars of 0.7–0.9 $M_\odot$ with $Z = 0.017 \times 10^{-4}$ to 0.0068, or $[{\rm Fe/H}] = -4.31$ to -0.71. They are shown in models of seven different metallicities. All metallicities appear in each panel. Evolutions for different masses (0.9, 0.85, 0.8, 0.75, and 0.7 $M_\odot$) are shown in different columns. As metallicity is reduced, the main-sequence life of a star of 0.8 $M_\odot$ is reduced from about 18 to about 12 Gyr. Varying metallicity also changes considerably $M_{\rm bcz}$, $T_{\rm bcz}$, and $T_{\rm eff}$. For instance, in 0.8 $M_\odot$ stars, the mass in the convection zone at an age of 12 Gyr is smaller by a factor of 10^4 in stars with $[{\rm Fe/H}] = -3.31$ as compared to that in stars with $[{\rm Fe/H}] = -0.71$, while the $T_{\rm eff}$ is 6700 K in the $[{\rm Fe/H}] = -3.31$ star but 5600 K in the $[{\rm Fe/H}] = -0.71$ star. The $M_{\rm bcz}$ is larger in the 0.9 $M_\odot$ star with $[{\rm Fe/H}] = -3.31$ than in the 0.7 $M_\odot$ star with $[{\rm Fe/H}] = -0.71$.

TABLE 1

COMPUTED MODELS

[Fe/H][a]	Z[b]	Y[c]	Mass ($M_\odot$)
−0.71	6.702×10^{-3}	0.243	0.50, 0.60, 0.70, 0.75, 0.80, 0.83, 0.85, 0.87, 0.90, 1.00, 1.20, 1.30
−1.31	1.676×10^{-3}	0.237	0.50, 0.60, 0.65, 0.70, 0.75, 0.80, 0.81, 0.82, 0.83, 0.85, 0.87, 0.90, 0.95, 1.00
−1.61	8.377×10^{-4}	0.236	0.50, 0.60, 0.70, 0.75, 0.78, 0.80, 0.82, 0.85, 0.90, 1.00
−2.01	3.351×10^{-4}	0.2354	0.50, 0.55, 0.60, 0.65, 0.70, 0.75, 0.77, 0.78, 0.785, 0.787, 0.79, 0.80, 0.81, 0.82, 0.83, 0.85, 0.90, 1.00
−2.31	1.676×10^{-4}	0.2352	0.50, 0.56, 0.58, 0.60, 0.70, 0.75, 0.77, 0.78, 0.782, 0.784, 0.79, 0.80, 0.81, 0.82, 0.83, 0.84, 0.85, 0.90, 1.00
−3.31	1.676×10^{-5}	0.23502	0.55, 0.60, 0.65, 0.70, 0.75, 0.76, 0.77, 0.78, 0.783, 0.785, 0.787, 0.79, 0.80, 0.83, 0.85, 0.90, 1.00
−4.41	1.676×10^{-6}	0.235002	0.70, 0.73, 0.75, 0.77, 0.80, 0.82, 0.85, 0.90

[a] Initial [Fe/H] value.

[b] Initial metals mass fraction (after α elements enhancement).

[c] Initial He mass fraction.

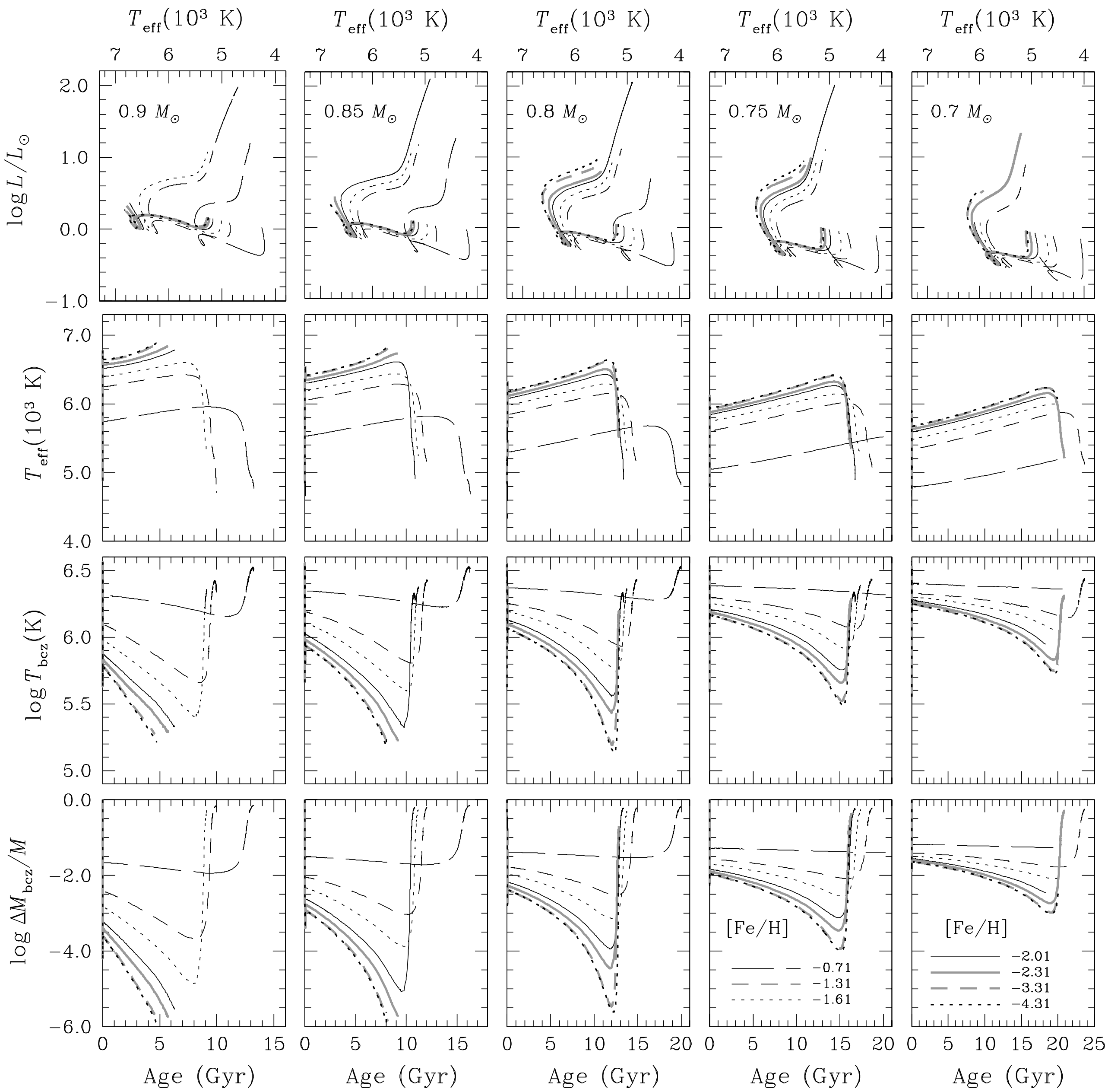

FIG. 1.—Hertzsprung-Russell diagram, and time evolution of $T_{\rm eff}$, temperature at the base of the surface convection zone ($T_{\rm bcz}$), and mass above the base of the surface convection zone ($M_{\rm bcz}$) of stars of 0.7–0.9 $M_\odot$ with $Z = 0.017 \times 10^{-4}$ to 0.0068, or [Fe/H] = −4.31 to −0.71. All models were calculated with atomic diffusion and radiative accelerations but no turbulent transport. The tracks in the HR diagram start at 2 Myr.

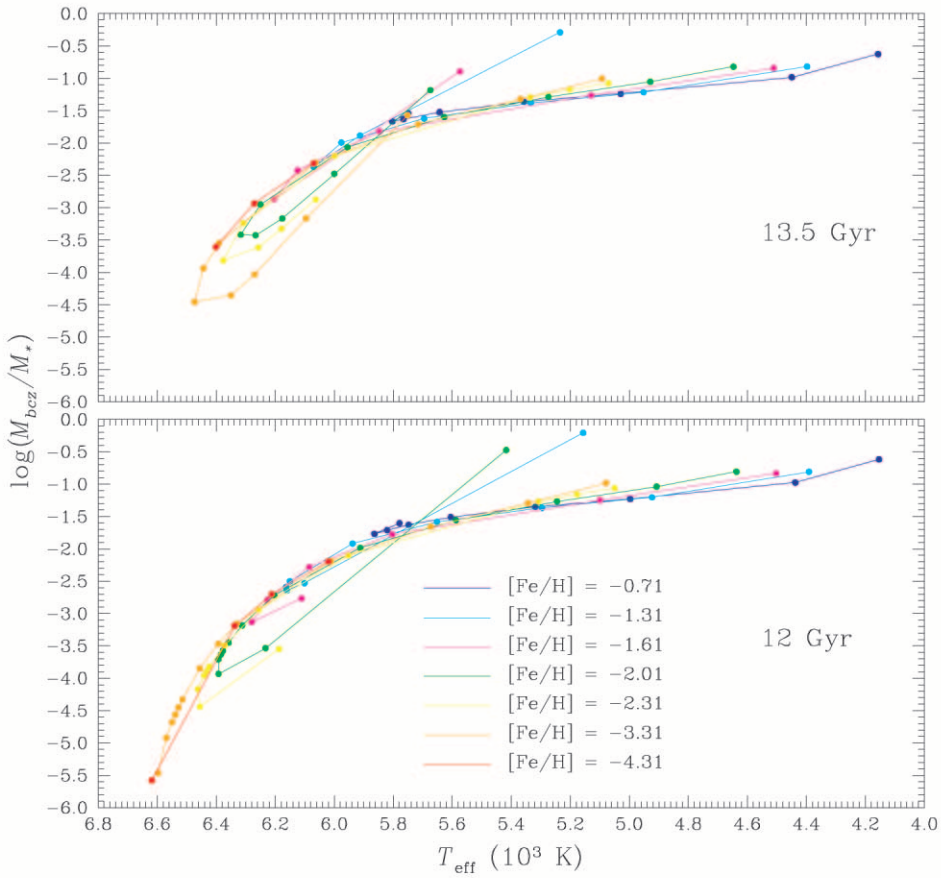

FIG. 2.—Mass above the base of the surface convection zone, M_{bcz}, of stars of 0.5 (rightmost end of each curve) to 1.2 $M_\odot$ with $Z = 0.017 \times 10^{-4}$ to 0.0068, or [Fe/H] = −4.31 to −0.71.

Whether one looks at the HR, T_{eff}, T_{bcz}, or M_{bcz}, one notes that the evolutionary curves are the same for [Fe/H] = −3.31 and −4.31. There are changes in global evolutionary properties as one reduces the metallicity from [Fe/H] = −2.31 to −3.31 but not as the metallicity is further reduced.

However, as seen in Figure 2, the reduction of the M_{bcz} with metallicity is essentially caused by the increase in T_{eff}. At a given T_{eff}, all main-sequence stars have very nearly the same M_{bcz}. As the metallicity is reduced, the star at a given T_{eff} has a smaller mass, but it has nearly the same M_{bcz}. However, if stars past the main-sequence turnoff are included, there is a wider spread in M_{bcz} at a given T_{eff}.

One may observe that lower metallicity clusters have turnoff stars with larger T_{eff} and that they have smaller M_{bcz}. The field halo stars with largest T_{eff} presumably have the smallest metallicity. Since atomic diffusion is much more effective if M_{bcz} is smaller, one expects larger effects of atomic diffusion in lower metallicity clusters.

Population I stars in the mass interval of AmFm stars have been shown by Richard et al. (2001) to develop Fe peak convection zones at $T = 200{,}000$ K. The only Population II stars that live more than 10 Gyr and whose surface convection zone has a T_{bcz} smaller than 200,000 K is the 0.8 $M_\odot$ star with [Fe/H] < 2.31 (see Fig. 1). It has been verified that it does not develop an iron peak convection zone. Its original Fe abundance is so small that Fe does not contribute substantially to opacity at $T = 200{,}000$ K even if, as seen below, it becomes overabundant by 1 dex during evolution.

3.2. *Radiative Accelerations*

The radiative accelerations below the surface convection zone play the most important role in determining the surface abundance variations. Their dependence on metallicity is shown in Figure 3 in 0.8 $M_\odot$ models of seven different metallicities. The g_{rad} are shown in each panel for stars of approximately the same age but of seven different metallicities.

The atomic configurations may be followed as the number of protons of the nucleus increases. Li is in the hydrogenic configuration at $\log \Delta M/M_* \approx -5$, whereas O is in that configuration at $\log \Delta M/M_* \approx -2$, and species from Ca to Fe are hydrogen-like at the center of the star. The configurations from Li to Ne dominate for O at $\log \Delta M/M_* \approx -5$, while for Fe they dominate at $\log \Delta M/M_* \approx -2$. Since the abundances of LiBeB are not varied with metallicity, their g_{rad} mainly vary because T, at a given $\log \Delta M/M_*$, increases as metallicity is decreased. This causes increased ionization and forces the peak g_{rad} of those species to move closer to the surface. The slight increase in the maximum of g_{rad}(B) is probably related to the increase in T_{eff} as metallicity is reduced (see Fig. 1). This

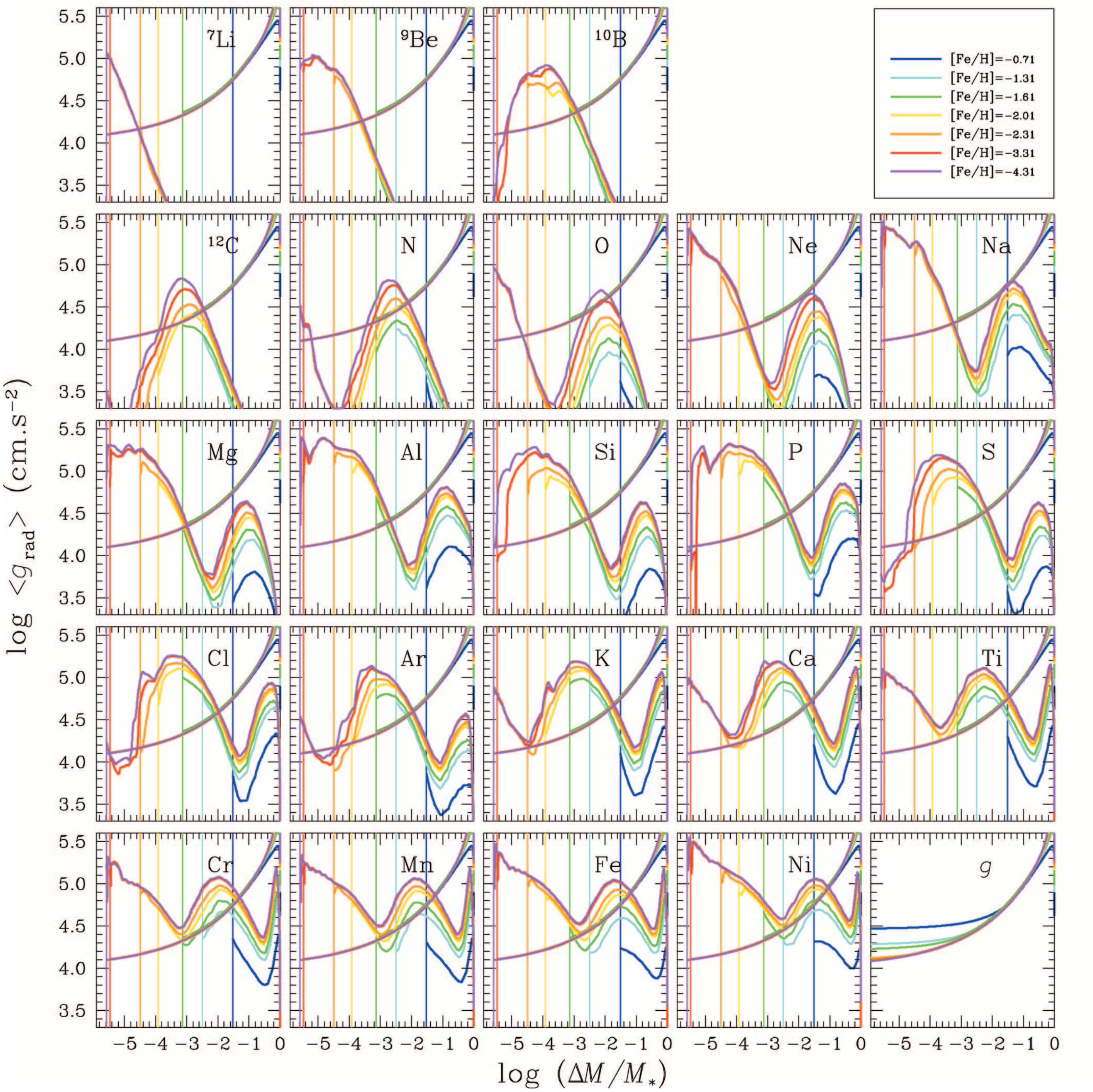

FIG. 3.—Radiative accelerations in Population II stars of 0.8 $M_\odot$ with [Fe/H] = −4.31 to −0.71 at an age of 12 Gyr. Gravity is shown in the lower right-hand corner and repeated in each part of the figure. The vertical lines give the position of the bottom of the surface convection zone for each metallicity; each curve is stopped at the corresponding line, for clarity. For other stellar masses, it is the position of the bottom of the convection zone that is most different. The g_{rad} of the various species are more sensitive to variations of metallicity than of mass or age. The depth of convection zones is more sensitive to changes of stellar mass, metallicity, and age than the g_{rad} are.

is indicative of the generalized g_{rad} increase caused by the T_{eff} variation.

A similar effect is present for heavier species, but then saturation also plays a role. For O, the position of the hydrogenic peak of g_{rad} shifts only from $\log \Delta M/M_* \approx -1.7$ to $\log \Delta M/M_* \approx -2.2$ as [Fe/H] varies from −4.31 to −0.71 but g_{rad}(O) varies by nearly a factor of 10 at its peak. At [Fe/H] = −3.31 the lines of hydrogenic O are essentially not saturated, and g_{rad}(O) is about equal to gravity. However, the lines of O are heavily saturated at [Fe/H] = −0.71, which causes a large g_{rad} reduction. Just as the H-like Li at $\log \Delta M/M_* \approx -5$, the g_{rad}(O) peak at $\log \Delta M/M_* \approx -2.2$ (where O is in LiBeB configurations) is strongly shifted toward the surface by the increased T caused by the lower [Fe/H]. For Mg, however, the shift toward the surface is compensated by the desaturation of the flux over the interval $-4 \le \log \Delta M/M_* \le -2$. Similarly, $g_{\rm rad}$(Fe) is hardly metallicity sensitive over the $-5 \le \log \Delta M/M_* \le -3$ interval where it is in configurations between Na and Ar. At $\log \Delta M/M_* \approx -1.5$, $g_{\rm rad}$(Fe) is about 3 times gravity at the lowest metallicities but about 3 times below gravity for [Fe/H] $= -0.71$.

At the lowest metallicities, one may note that some of the $g_{\rm rad}$ curves become noisy [in particular $g_{\rm rad}$(Si)] because of the undersampling of frequencies for the $g_{\rm rad}$ calculations (see Richer et al. 1998). We do not believe that any of the results presented in this paper are significantly affected by this.

At [Fe/H] $= -0.71$ and -1.31, the models go through regions of the ρ-T plane where atomic data were not available to us to calculate $g_{\rm rad}$ of a few species (P, Cl, K, Ti, Cr, Mn, and Ni). Since this only occurred in convection zones, where there is no significant abundance stratification, it did not affect the diffusion calculations. It is the reason why $g_{\rm rad}$ are not shown in convection zones.

As seen in Figure 2 of Paper I for [Fe/H] $= -2.31$, the values of $g_{\rm rad}$ do not vary considerably with the age of the star. At other metallicities, the $g_{\rm rad}$ have similar time dependence (not shown). It is the reduction of $M_{\rm bcz}$ with age that causes Fe, for instance, to be supported when stars are close to the turnoff but not earlier (see also Fig. 2 and the related discussion for the link with $T_{\rm eff}$). Whether Fe is supported close to the turnoff depends on how superficial the convection zone becomes at turnoff. This varies strongly with M_* and metallicity as seen in Figure 1. As seen in Figure 3, $g_{\rm rad}$(Fe) is larger than gravity below the convection zone for [Fe/H] ≤ -2.01 but not for larger metallicities. As seen below, this leads to overabundances of Fe for [Fe/H] ≤ -2.01 at 12 Gyr. At 13.5 Gyr, the limit is [Fe/H] $= -2.31$ because, at that age, the 0.8 $M_\odot$ star has evolved past turnoff where the increased $M_{\rm bcz}$ causes $g_{\rm rad}$(Fe) to be smaller. The $g_{\rm rad}$ of many species are larger than gravity, below the convection zone, for a significant fraction of the star's life for models with [Fe/H] ≤ -2.01.

3.3. *Evolution of Surface Abundances*

The time variation of surface abundances in Population II stars with atomic diffusion is shown in Figure 4 for [Fe/H] $= -3.31$. A vertical cut through each set of curves shows the range of anomalies to be expected at a given age in a cluster. As the cluster ages, the range of abundance anomalies is reduced, since the more massive stars, which have the larger anomalies, evolve away from the main sequence. Figure 4 may be compared with Figure 3 of Paper I, where similar results are shown for a cluster with [Fe/H] $= -2.31$. Comparing the two figures, one first notes their considerable similarity. The same species are over- or underabundant by similar factors although at slightly different ages. If one compares carefully, one notes a shift of approximately 2 Gyr, in that the anomalies to be expected at $t = 13.5$ Gyr in a cluster with [Fe/H] $= -2.31$ are seen at $t = 15.5$ Gyr in a group of stars with [Fe/H] $= -3.31$. At 12 Gyr, the maximum Fe overabundance may attain a factor of 100 if [Fe/H] $= -3.31$ but is limited to a factor of 10 if [Fe/H] $= -2.31$. The abundance variations seen at 12 Gyr in [Fe/H] $= -2.31$ stars are still present at 14 Gyr if [Fe/H] $= -3.31$.

The surface abundances reflect the variation of $g_{\rm rad}$ below the surface convection zone as the bottom of the convection zone moves toward the surface. This is especially noteworthy for Li in the 0.8 $M_\odot$ model, whose abundance progressively decreases to a factor of 10 underabundance at 10.8 Gyr, then has a maximum at 12 Gyr when, just after turnoff, the Li abundance is only a factor of 2 smaller than the original abundance, then briefly decreases to an underabundance by a factor of 20 at 12.5 Gyr as the convection zone starts expanding at the beginning of the subgiant branch, and back to a factor of only 1.4 underabundance at 12.7 Gyr at the bottom of the red giant branch ($T_{\rm eff} \simeq 5600$ K). The maximum at 12 Gyr in the Li abundance occurs as the $M_{\rm bcz}$ is close to its minimum value, which is close to the value shown in Figure 3 by the vertical line; in that figure, $g_{\rm rad}$(Li) is seen to be larger than gravity below the convection zone. One may note the simultaneous mirror behavior of S, whose $g_{\rm rad}$ has a minimum below the convection zone at 12 Gyr (see Fig. 3) and whose abundance has a minimum at 12 Gyr in the 0.8 $M_\odot$ model (see Fig. 4).

The difference in the behavior of He and Li in Figure 4 is striking. Helium has much larger underabundances than Li. We have verified that He and Li have very similar *settling* velocities (not shown). The striking difference in their behavior comes from our taking into account $g_{\rm rad}$(Li) in the diffusion equation. Even when $g_{\rm rad}$(Li) does not cause surface Li overabundance, its strength below the surface convection zone is sufficient to considerably reduce Li underabundances. One may also note that the effect of $g_{\rm rad}$(Be) and $g_{\rm rad}$(B) is even larger.

4. METALLICITY DEPENDENCE OF ABUNDANCE ANOMALIES

The surface concentrations of the 28 calculated species potentially impose constraints on stellar models. In order to permit comparisons to observations, they are presented as both a function of atomic number in given stars and a function of $T_{\rm eff}$ at given evolutionary ages. They are shown for [Fe/H] $= -4.31$ to -0.71. All models were calculated with atomic diffusion and radiative accelerations but no turbulent transport.

4.1. *As a Function of Atomic Number*

The surface concentrations[2] in turnoff stars of various metallicity ([Fe/H] from -3.31 to -0.71) are shown as a function of atomic number in Figure 5. They are shown at the surface of the star with highest $T_{\rm eff}$ at 13.5 Gyr for each metallicity. As seen below, this is not necessarily the star with largest abundance anomalies, but it is representative of stars with large anomalies in each case. In a cluster with [Fe/H] $= -0.71$, most species have nearly the same underabundance factor of -0.14 dex. The only significantly different values are for He, Li, and Be, for which the mass difference between isotopes plays a role. As the metallicity is reduced, the $T_{\rm eff}$ of the hottest turnoff star increases (see Figs. 1 and 2), the $M_{\rm bcz}$ progressively decreases, and the effect of $g_{\rm rad}$ becomes visible in surface abundances. One

[2] The surface concentrations of metals in this and most following figures are given with respect to the hydrogen concentration. Part of the [Fe/H] variation, for instance, comes from He settling. This is fully included in the calculations. When large He abundance changes occur there are also significant Fe ones so that its effect is always relatively small. In a 1.0 dex change of [Fe/H], 0.15 dex may come from He settling. We have chosen to present [Fe/H] in most figures since that is what is usually measured.

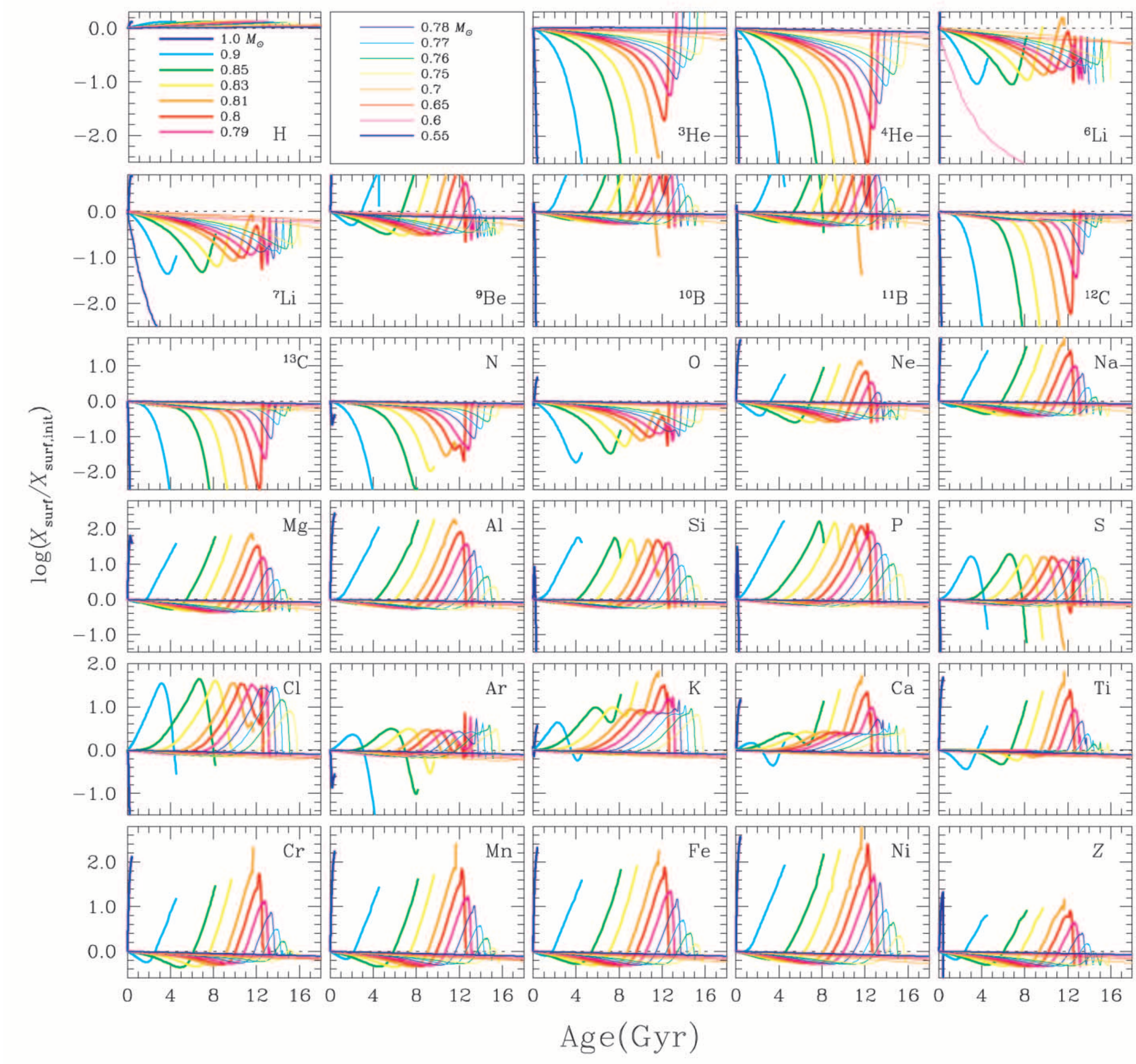

FIG. 4.—Surface abundance variations in Population II stars of 0.5–1.0 $M_\odot$ with [Fe/H] $= -3.31$. A vertical cut through each set of curves permits an evaluation of the range of surface abundances of a species at one age in the cluster.

then sees the progressive shift in the atomic shell (Li- to F-like) as Ca, K, and Cl are, respectively, the most overabundant species at [Fe/H] $= -1.3$, -1.61, and -2.31. Simultaneously, B and Ni are progressively more supported as other atomic shells also play a role: the hydrogenic configuration for B and the Na/Mg configurations for Ni.

To illustrate how anomalies vary with evolutionary age around turnoff, the surface abundances in stars of 0.75–0.80 $M_\odot$ of [Fe/H] $= -2.01$ are shown in Figure 6 at 13.5 Gyr and in Figure 7 at 13.0 Gyr. At 13.5 Gyr, the hottest star ($T_{\rm eff} = 6317$ K; $M = 0.77$ $M_\odot$) is not the one with the largest anomalies, which is the $T_{\rm eff} = 6267$ K, $M = 0.78$ $M_\odot$ one, even if it is past turnoff. The slightly pre-turnoff 0.75 $M_\odot$ star at $T_{\rm eff} = 6250$ K has very nearly the same anomalies as the post-turnoff 0.787 $M_\odot$ star at $T_{\rm eff} = 6000$ K. By the time a star reaches $T_{\rm eff} = 5674$ K, all species from C to Ni have about the same 0.1 dex underabundance while Li starts being affected by nuclear burning. The shifts in the atomic number of supported species occur in a way very similar to that seen in Figure 5.

When the cluster is 0.5 Gyr younger (Fig. 7), the 0.79 $M_\odot$ star has the largest anomalies. Both its over- and underabundances are larger by 0.1 dex than the anomalies in the $M = 0.78$ $M_\odot$ star at 13.5 Gyr. The surface abundances in the subgiant 0.80 $M_\odot$ star at $T_{\rm eff} = 5506$ K, are also shown. At that $T_{\rm eff}$, underabundances have been reduced by dredge up to 0.05 dex for most species. The exceptions are Li and Be, which are affected by nuclear burning and ^{3}He, which

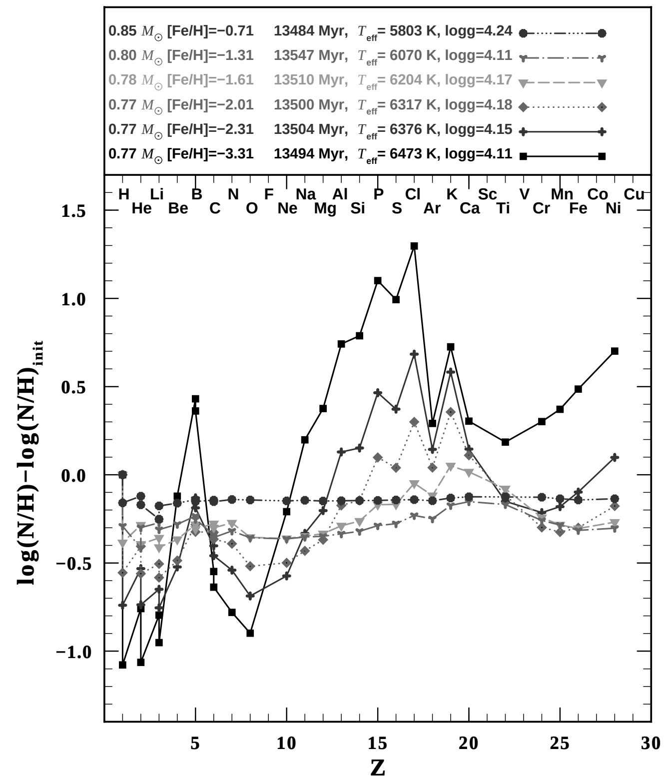

FIG. 5.—Surface abundances in Population II stars at turnoff at an age of 13.5 Gyr, normalized to the original abundances. Models with [Fe/H] $= -3.31$ to -0.71 are shown. 28 different species are shown. Along each curve, the lighter isotopes come first, for species for which more than one isotope was included (H, He, Li, B, and C). The same original abundance was used for Li, Be, and B, independent of metallicity. For each metallicity, the star with largest $T_{\rm eff}$ was chosen.

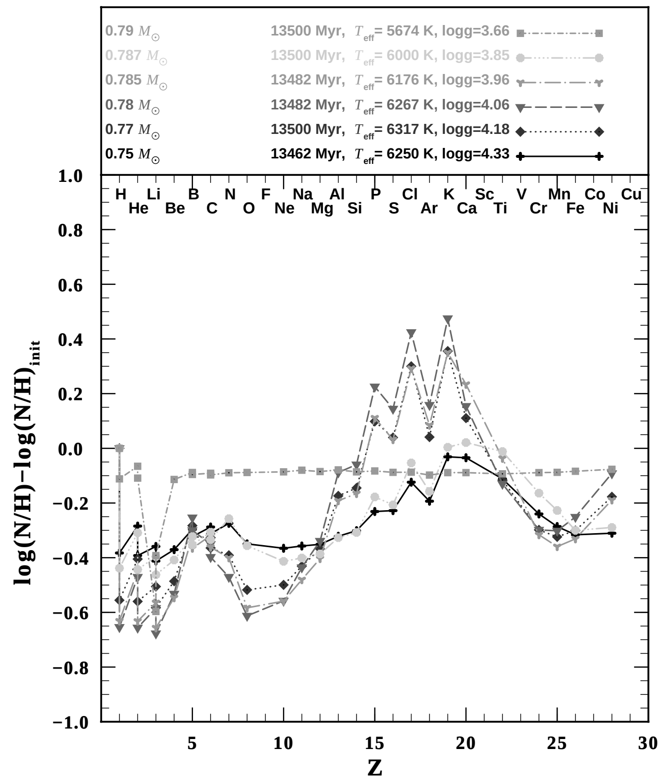

FIG. 6.—Surface abundances, normalized to the original abundances, in Population II stars around turnoff at an age of 13.5 Gyr in a cluster with [Fe/H] $= -2.01$.

has been produced by nuclear reactions. Note that there remains a general 0.05 dex underabundance even when the mixed region is large enough for surface abundances of Li, Be, and ^{3}He to have been affected by nuclear reactions.

The time evolution of the surface abundance anomalies around turnoff are shown in Figure 8 as a function of Z for a 0.77 $M_\odot$ star of [Fe/H] $= -3.31$. Eight evolutionary times are shown. Anomalies are larger in this very low metallicity star than in a [Fe/H] $= -2.01$ cluster (Fig. 6). Overabundances reach a factor of 20 for Cl at maximum, while underabundances reach a factor of 10 for He, Li, and O. The largest anomalies are for species between Mg and Ca. Such Z dependence of anomalies leads to scatter when observations are presented in the form of [X/Fe] as a function of [Fe/H] for field stars such as in Figures 5–8 of Norris et al. (2001). Note that the largest anomalies are not when the star has the largest $T_{\rm eff}$ but rather slightly past turnoff. This point is further discussed in the next section.

4.2. *As a Function of* $T_{\rm eff}$

Isochrones of abundances normalized to hydrogen, $[N(X)/N(H)]$, as a function of $T_{\rm eff}$ were shown at 12 and 13.5 Gyr in Figures 13 and 14, respectively, of Paper I for clusters with [Fe/H] $= -2.31$; in Paper I, some evolutionary models were calculated with atomic diffusion only, but in others turbulence was also included. Here similar isochrones are shown at 12 Gyr (Fig. 9) for a number of metallicities; the stellar evolution calculations are all with atomic

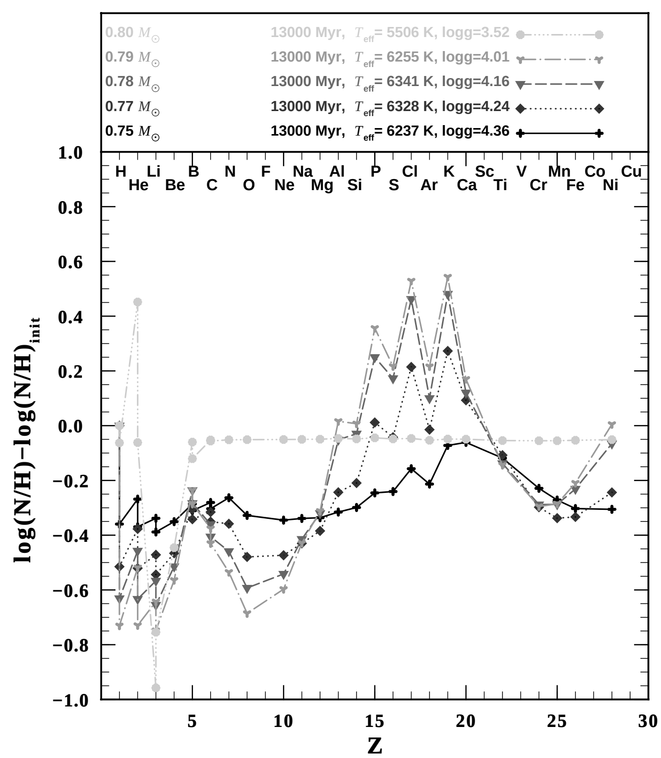

FIG. 7.—Surface abundance, normalized to the original abundances, in Population II stars around turnoff at an age of 13.0 Gyr in a cluster with [Fe/H] $= -2.01$.

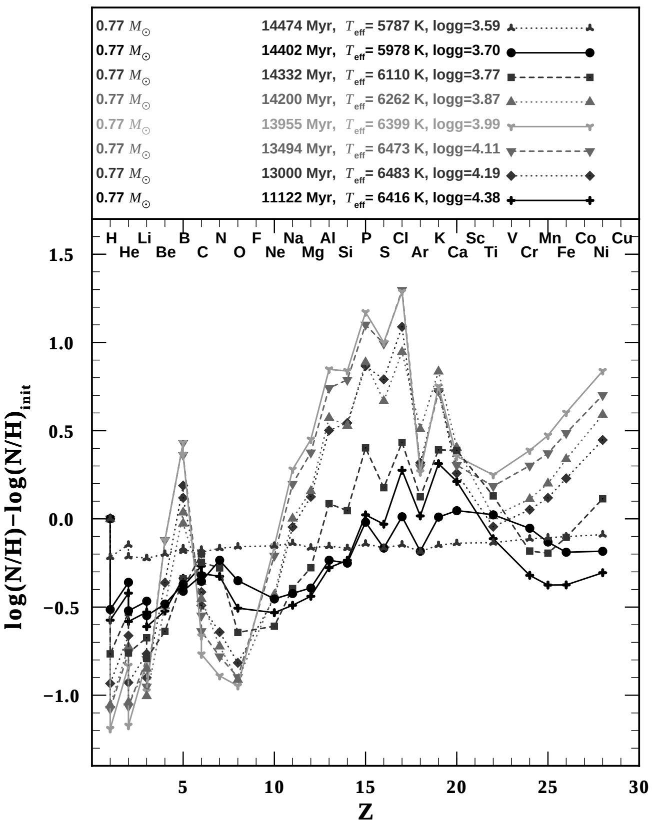

FIG. 8.—Surface abundance, normalized to the original abundances, in a 0.77 $M_\odot$ Population II star of [Fe/H] $= -3.31$. The results are shown at eight ages as the star evolves around turnoff.

diffusion and without turbulence. At 13.5 Gyr (Figs. 10 and 11), isochrones of the abundances normalized to H are shown for Fe and LiBeB only, while all other isochrones are for abundances with respect to the Fe abundance, [N(X)/N(Fe)], in order to facilitate comparison with observations.

The 12 Gyr surface abundance isochrones are shown as a function of $T_{\rm eff}$ for 16 species in Figure 9. In stars with $T_{\rm eff} \leq 6000$ K, there are underabundances by 0.1–0.2 dex for all species, the largest underabundances occurring in those stars with the smallest metallicity and closest to 6000 K. At 12 Gyr, all stars with original [Fe/H] $= -0.71$ have $T_{\rm eff} \leq 6000$ K, so that atomic diffusion leads to generalized underabundances in clusters with that metallicity. They are by approximately 0.1 dex. In a cluster with [Fe/H] $= -1.31$, there are stars up to approximately 6200 K. The effect of $g_{\rm rad}$ is seen on the abundances in the few hottest stars and most clearly for Cl and Ca (which is the only species to become overabundant) although one may also notice it for C, Si, S, and Cr. Most other species are also affected by having smaller underabundances than would be the case in the absence of $g_{\rm rad}$. The underabundances are by a larger factor than in stars with [Fe/H] $= -0.71$ even if $g_{\rm rad}$ reduces underabundances for most species.

In clusters with [Fe/H] $= -2.01$, there are turnoff stars with $T_{\rm eff}$ up to 6400 K; in these, species from Al to Ca as well as Ni are overabundant. At turnoff, the Fe abundances are between their original value and 0.3 dex below. This abundance spread is seen at 6400 K but has practically disappeared at 6200 K and so is limited to a very narrow $T_{\rm eff}$ range.

Abundance variations at turnoff are large for many species when [Fe/H] ≤ -2.01, but those variations disappear for [Fe/H] between -2.01 and -1.31. They are, on the contrary, larger in clusters with [Fe/H] $= -2.31$ (see Paper I) and even larger when [Fe/H] $= -3.31$. In the latter case, turnoff stars have $T_{\rm eff}$ between 6400 and 6600 K. The surface convection zone is 10 times less massive than in a cluster with [Fe/H] $= -2.31$ (Fig. 2). The $g_{\rm rad}$ are consequently larger immediately below the surface convection zone (by about 0.3 dex for Fe in a 0.8 $M_\odot$ star; see Fig. 3), and the diffusion timescales are consequently shorter, leading to larger overabundances. In the most metal-poor stars of 6600 K, Li, Be and B are supported by their $g_{\rm rad}$. This causes the Li concentration to be brought back to nearly its original value, while Be and B are overabundant by factors of up to 10.

At 13.5 Gyr, Figure 10 shows that [Fe/H] is reduced by settling by about 0.1 dex at $T_{\rm eff} = 5000$ K irrespective of metallicity. This reduction increases to about 0.2 dex, again irrespective of metallicity, at $T_{\rm eff} = 5800$ K. This follows from Figure 2 since, before turnoff, $M_{\rm bcz}$ depends only on $T_{\rm eff}$ and not on metallicity. At a given age, the settling is consequently about the same in all main-sequence stars of a given $T_{\rm eff}$. The one exception is at $T_{\rm eff} = 5800$ K, in the model with [Fe/H] $= -0.71$, where the reduction is by 0.15 dex instead of 0.2 dex because of the slightly larger $M_{\rm bcz}$ in that model (see Fig. 2). Above $T_{\rm eff} = 5800$ K, the anomalies are still largely independent of metallicity so long as settling dominates. However, as $T_{\rm eff} = 6000$ K is approached, $g_{\rm rad}$ starts playing a role, and even small differences in $M_{\rm bcz}$ *and* $T_{\rm bcz}$ become important, so that there is more variation from star to star and between clusters of different metallicities. One additional reason is that, at a given $T_{\rm eff}$ and after turnoff, stars have $M_{\rm bcz}$ that are significantly different from those before turnoff (see Fig. 12). For instance, at 6300 K, a 0.8 $M_\odot$ star has $\log(M_{\rm bcz}/M_*) = -2.9$ before turnoff but -3.6 after turnoff. Stars whose $T_{\rm eff}$ becomes larger than 6000 K have a smaller $M_{\rm bcz}$ immediately after turnoff (until they reach 5900 K). Their [Fe/H] increases during turnoff, leading to the appearance of loops in Figure 10. Large [Fe/H] variations in turnoff stars are limited to clusters with [Fe/H] ≤ -2.31. They disappear for clusters with [Fe/H] between -2.31 and -2.01. As the metallicity is increased from [Fe/H] $= -2.31$ to -2.01, the $M_{\rm bcz}$ increases sufficiently, even at turnoff, for Fe to cease being supported sufficiently by $g_{\rm rad}$(Fe) below the convection zone to cause increases in X(Fe). However, $g_{\rm rad}$(Fe) still reduces gravitational settling significantly at those $T_{\rm eff}$. As they cool beyond $T_{\rm eff} = 5900$ K, all stars have larger $M_{\rm bcz}$ after than before turnoff; as they move toward the giant branch, their convection zones become much more massive.

One notes that the overabundances are much smaller at 13.5 than at 12 Gyr. This is linked to the maximum $T_{\rm eff}$ at turnoff that goes down as clusters age. Turnoff stars with nearly normal Li abundance are seen at 12 Gyr but not at 13.5 Gyr.

As seen in Figure 11, up to $T_{\rm eff} = 5800$ K, all metals (that is, excluding LiBeB) vary like Fe. Variations with respect to Fe appear only at the level of approximately 0.02 dex. The small variations may be linked to small differences in atomic and thermal diffusion coefficients caused by the different atomic mass and degree of ionization among species. For $T_{\rm eff} \geq 5800$ K, large variations appear. One sees the effect of atomic shells being successively important, as CNO set-

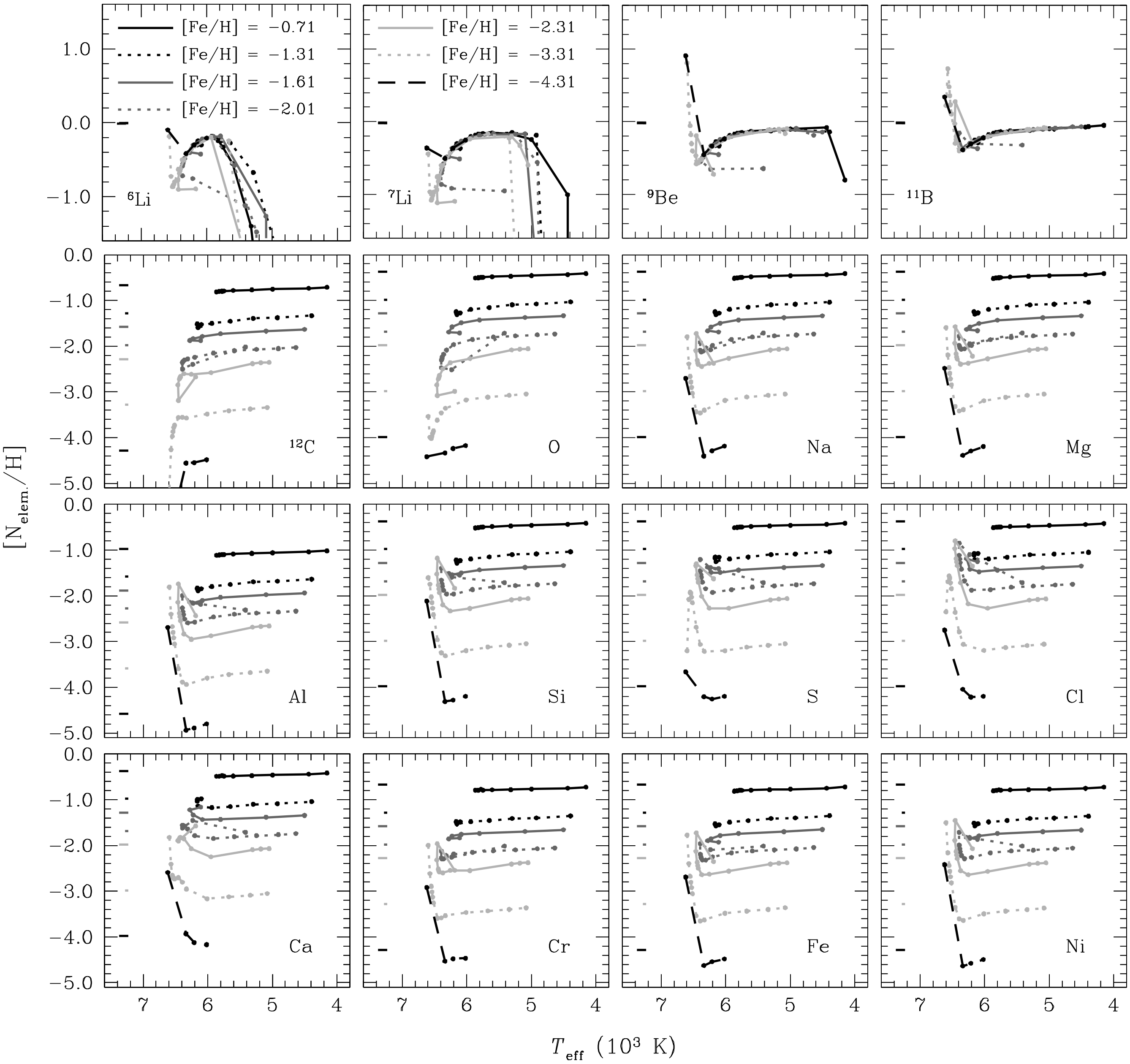

FIG. 9.—Surface abundance isochrones in Population II stars of 0.5–1.2 $M_\odot$ at an age of 12 Gyr. Series of models were calculated with [Fe/H] $= -4.31$ to -0.71. For [Fe/H] $= -4.31$, models were calculated for only a few masses. Twenty-eight different species were followed in the calculations, although only 16 are shown. The starting abundances for Li, Be, and B were not varied with metallicity. The starting abundances are indicated by a short horizontal line close to the left-hand scale. [*See the electronic edition of the Journal for a color version of this figure.*]

tles much more than Fe (they have smaller $g_{\rm rad}$), Na and Mg are slightly less supported than Fe, and the overabundances are progressively larger up to Cl; Cl is up to 10 times more overabundant than Fe. Ca and Cr have a complex behavior, while Ni is more overabundant than Fe. The time dependence of the abundances normalized to Fe is complicated by the time dependence of the Fe abundance that depends on the $\log \Delta M/M_*$ dependence of $g_{\rm rad}$(Fe).

For many species the $\log \Delta M/M_*$ dependence of $g_{\rm rad}$ differs from that of $g_{\rm rad}$(Fe) (see Fig. 3). It leads to different layered structures for different chemical species. The $\log \Delta M/M_*$ dependence of X(C), X(O), X(Ca), and X(Fe) in 0.77 $M_\odot$ models with metallicity of [Fe/H] $= -2.01$ (*upper row*) and -3.31 (*lower row*) is shown in Figure 13 at a few evolutionary ages around turnoff. These constitute a typical sample of the 28 species whose concentration was followed in detail. In the lower metallicity case, one notes maxima in $X(^{12}{\rm C})$ and X(Ca) at $\log \Delta M/M_* \simeq -3.7$. The $g_{\rm rad}$(Ca) is larger than $g_{\rm rad}$(C) (see Fig. 3), but both peak at $\log \Delta M/M_* \simeq -3.1$. The larger $g_{\rm rad}$(Ca) leads to a stronger abundance peak for Ca than $g_{\rm rad}$(C) for C, and the Ca overabundance extends into the surface convection zone at many evolutionary phases when C is underabundant. At $T_{\rm eff} = 5900$ K (14.42 Gyr), the surface C is 0.2 dex underabundant, while $g_{\rm rad}$(Ca) still keeps the Ca abundance equal to the original one. Fe is supported by $g_{\rm rad}$ immediately below the convection zone, and its maximum abundance is in the surface convection zone. As evolution proceeds and

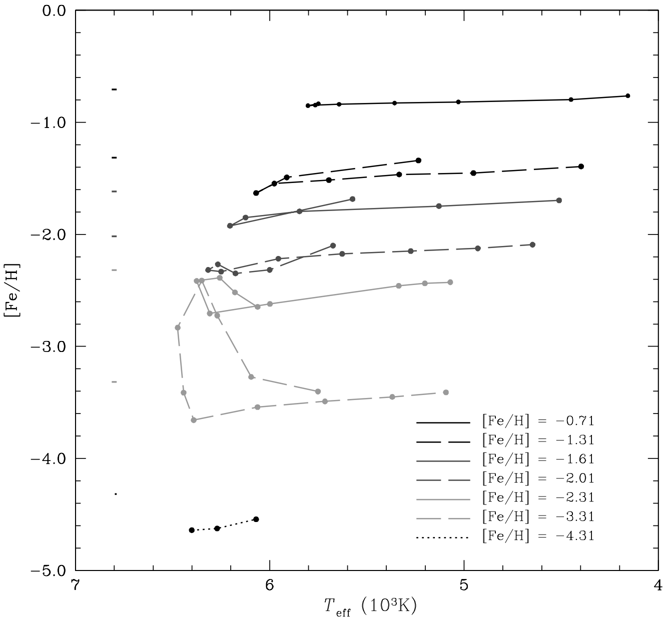

FIG. 10.—Surface abundance isochrones of Fe in Population II stars of 0.5–1.2 $M_\odot$ at an age of 13.5 Gyr. Series of models were calculated with $[\mathrm{Fe/H}] = -4.31$ to -0.71. For $[\mathrm{Fe/H}] = -4.31$, models were calculated for only a few masses. The points of the series with $[\mathrm{Fe/H}] = -2.01$ are for 0.79, 0.787, 0.785, 0.78, 0.77, 0.75, 0.70, 0.65, 0.60, 0.55, and 0.50 $M_\odot$. The hottest star is the 0.77 $M_\odot$ one. Initial values are shown by short lines on the left.

the convection zone becomes deeper, this leads to the complicated behavior shown in Figure 11, since the surface Fe overabundance is diluted into a more massive zone while the Ca abundance peak leads, when the bottom of the convection zone crosses it, to an increase of the surface Ca abundance. This complicates the [Ca/Fe] isochrone. Other species, such as Cr for instance, have similar behavior. The time dependence of the O abundance is simpler as it is not supported in the exterior regions. Its $g_{\rm rad}$ is comparable to gravity only at $\log \Delta M/M_* \simeq -2$. It slows O settling there but this does not influence the surface O abundance much. In the model with $[\mathrm{Fe/H}] = -2.01$, the highest $T_{\rm eff}$ reached is smaller, the convection zone is consequently deeper, and, at its bottom, the $g_{\rm rad}$ are smaller. The effects on surface concentration, while present, are smaller. The $g_{\rm rad}$ considerably reduces the settling of C and Fe but without leading to an overabundance of Fe. Only Ca becomes overabundant, but by a factor of 3 times smaller than in the $[\mathrm{Fe/H}] = -3.31$ model.

5. COMPARISON TO ABUNDANCES IN GLOBULAR CLUSTERS

We compare the abundance isochrones of models of different metallicities to a number of clusters in which turnoff stars were recently observed. The comparison is presented in order of increasing metallicity. Since in this paper results are presented for stars with $Z = 0.017 \times 10^{-4}$ to 0.0068, we will compare with the abundance determinations in M92, NGC 6397, and M71. We do not compare our results with the observations of NGC 6752 where the relatively large abundance variations observed in giants complicates the interpretation of turnoff stars observations.

5.1. *M92*

Comparison of our calculations to abundance observations of M92 (King et al. 1998, $[\mathrm{Fe/H}] = -2.31$) have already been presented in Paper I and its age determined as 13.5 Gyr in VandenBerg et al. (2002, hereafter Paper II). It was shown in Paper I that observed star-to-star abundance variations in some turnoff stars were similar to those expected from atomic diffusion if the real $T_{\rm eff}$ of the observed stars were some 100 K higher than the observationally determined $T_{\rm eff}$. As seen in Figure 10, the observed variations of [Fe/H] are expected at and past turnoff at the metallicity of M92 but *not* in clusters with larger metallicities.

5.2. *NGC 6397*

There are a number of abundance determinations in giant stars of NGC 6397 (Zinn & West 1984; Minniti et al. 1993; Carretta & Gratton 1997; Castilho et al. 2000). Castilho et al. (2000) obtain $[\mathrm{Fe/H}] = -2.00$ with an rms dispersion of ± 0.05 irrespective of position in the HR diagram. Their stars cover the interval from $T_{\rm eff} = 4150$ K, $\log g = 0.60$ to $T_{\rm eff} = 5545$ K, $\log g = 3.30$ with only two stars above 5400 K. Gratton et al. (2001) obtain $[\mathrm{Fe/H}] = -2.05$ for their three stars at the base of the giant branch ($T_{\rm eff} = 5478$ K, $\log g = 3.42$). Zinn & West (1984) had obtained $[\mathrm{Fe/H}] = -1.91$, and Carretta & Gratton (1997) $[\mathrm{Fe/H}] = -1.82 \pm 0.04$. The observed [Fe/H] from −2.05 to −1.82 implies significant differences between authors. The observed differences are largely explained by the error bars quoted by the various authors for $T_{\rm eff}$ and in particular for the $T_{\rm eff}$ scales.

There are two abundance determinations in turnoff stars of NGC 6397 (Thévenin et al. 2001; Gratton et al. 2001; $[\mathrm{Fe/H}] = -2.02$ and −2.03, respectively). Both the LTE and non-LTE (NLTE) parameters determined by Thévenin et al. (2001) are shown in Figure 14. Following Thévenin & Idiart (1999), they obtained $\log g$ and [Fe/H] by forcing Fe I and Fe II to lead to the same Fe abundance. They used both LTE and NLTE models for Fe. The NLTE [Fe/H] of the turnoff stars of NGC 6397 included in the sample of Thévenin et al. (2001) vary from −2.05 to −2.01. Their turnoff subgiants have from $T_{\rm eff} = 6075$ K, $\log g = 4.05$ to $T_{\rm eff} = 6330$ K, $\log g = 4.25$. They evaluate abundance error bars of 0.1 dex from atmospheric parameters uncertainty but obtain a smaller dispersion (0.04; see their Table 3) than this for [Fe/H]. Such a consistency is obtained after correcting atmospheric parameters. For other metals, in their Table 6, Thévenin et al. (2001) give 0.25 dex for [Ca/Fe], and less than 0.1 dex for [Mg/Fe] and [Na/Fe]. They mention that these ratios are consistent with those observed in giants by Castilho et al. (2000).

In their analysis of turnoff and subgiant stars of NGC 6397, Gratton et al. (2001) adopted one single set of atmospheric parameters for each group. For their turnoff stars they determined $T_{\rm eff} = 6476$ K, $\log g = 4.10$. They give, averaged over both groups, a value for $[\mathrm{Fe/H}] = -2.04$. They do not give $T_{\rm eff}$ and $\log g$ values for individual cluster stars, but they do give abundances for individual stars. From their Table 2, in turnoff stars, [Fe/H] varies from −2.00 to −2.06, while in subgiants, it goes from −2.01 to −2.10; for [O/Fe], it is, respectively, 0.08–0.21 and 0.26–0.48; for [Na/Fe], it is, respectively, 0.02–0.28 and 0.21–

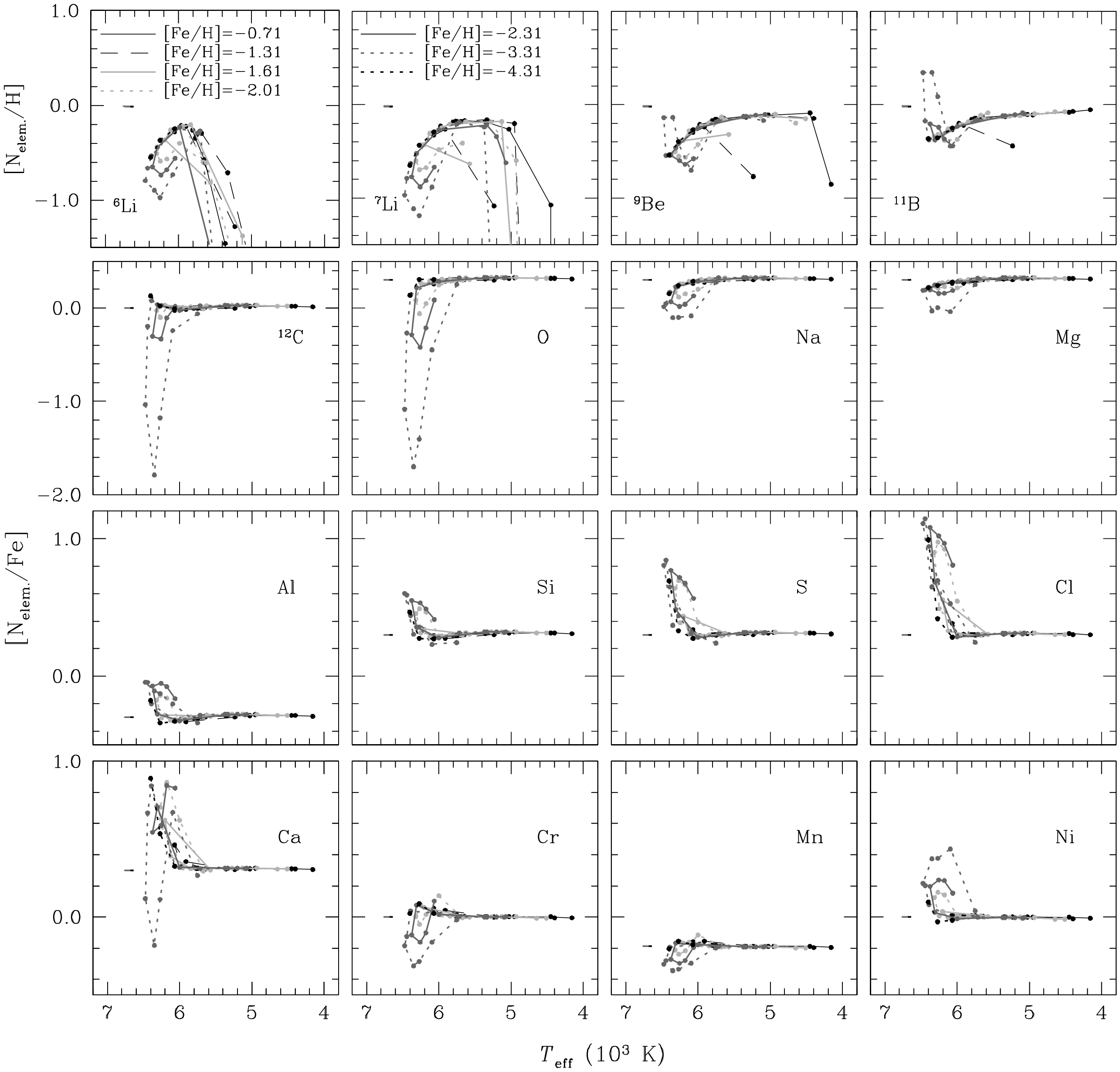

FIG. 11.—Surface abundance isochrones in Population II stars of 0.5–1.2 $M_\odot$ at an age of 13.5 Gyr. Twenty-eight different species were followed in the calculations although only 16 are shown. The [Fe/H] isochrones are shown on Fig. 10. The same original abundances were used for Li, Be, and B independent of metallicity. The starting abundance is indicated by a short horizontal line close to the left-hand scale. Note that the LiBeB concentrations are normalized to H, while the others are normalized to Fe. [*See the electronic edition of the Journal for a color version of this figure.*]

0.48; for [Mg/Fe] it is, respectively, −0.06 to 0.12 and 0.10–0.28; finally, for [Al/Fe] it is 0.10–0.26 and 0.28–0.46.

Among the various turnoff stars observed, both Gratton et al. (2001) and Thévenin et al. (2001) obtain the same [Fe/H] within 0.06 dex. Over the same $T_{\rm eff}$ range, one expects a range of 0.1 dex for variations of [Fe/H] for our post-turnoff stars in a cluster with [Fe/H] = −2.01 (see Fig. 10). This discrepancy seems marginally significant.

In comparing the [X/Fe] calculated in our models to observations, there is acceptable agreement with Gratton et al. (2001). The values they obtained for [O/Fe], [Na/Fe], and [Mg/Fe] are consistent with Figure 11, while their [Al/Fe] is in the opposite direction.

The constancy of the [X/Fe] ratios for turnoff *and* giants claimed by Thévenin et al. (2001) would be a serious difficulty since according to Fig. 11, [Ca/Fe] could be overabundant by up to 0.9 dex in some turnoff stars compared to giants.

According to the calculations presented in this paper, for a cluster with [Fe/H] = −2.01 and an age of 13.5 Gyr (see Fig. 10 and the discussion of § 4.2), one expects a 0.2 dex lower [Fe/H] in turnoff than in giant stars. This would be consistent with the NLTE [Fe/H] = −2.01 value for turnoff stars if one accepts the larger abundances determined for Fe in giants (Zinn & West 1984; Carretta & Gratton 1997). It would also be consistent with the LTE [Fe/H] and the lower subgiant [Fe/H] of Gratton et al. (2001) as seen in Figure 14. In this figure, one also sees that the NLTE [Fe/H] would be consistent with the lower subgiant [Fe/H] of Gratton et al. (2001) if the cluster were 12 Gyr old.

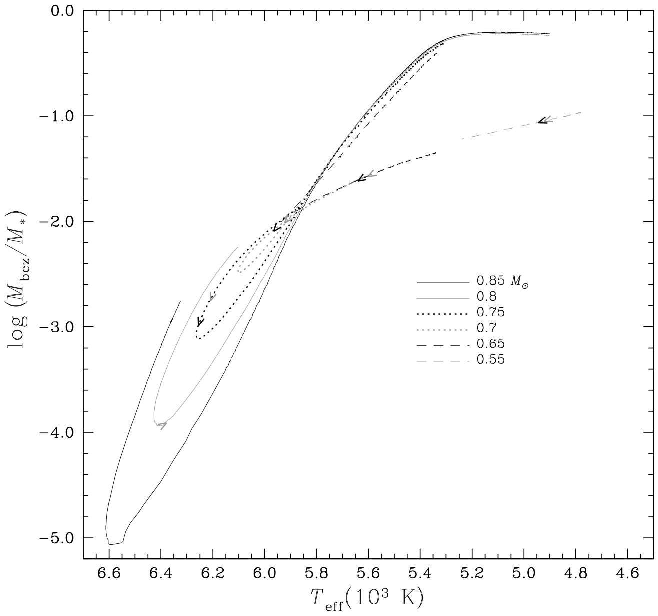

FIG. 12.—Evolution of $M_{\rm bcz}$ as a function of $T_{\rm eff}$ in Population II stars with [Fe/H] $= -2.01$ and ranging in mass from 0.5 to 0.85 $M_\odot$. The tracks were started after 100 Myr of evolution in order to reduce the complexity of the figure. Stars of 0.7 $M_\odot$ and more start their evolution descending on the appropriate left section ($T_{\rm eff} > 6000$ K) of each curve and loop upward to the right. Stars of 0.65 $M_\odot$ and less make no such loop. Arrows point in the direction of evolution. Gray arrows identify stars at 12 Gyr and black arrows at 13.5 Gyr.

When one does a detailed comparison of the observations of other metals (including error bars) with our models, there is potential agreement. The Na and Mg variations, for which Thévenin et al. (2001) include observations in turnoff and subgiant stars, are consistent with our isochrones within error bars (see Fig. 14). While they do not include values in subgiants for Ca, Ti, Cr, and Ni, the values given for turnoff stars would be consistent with the isochrones, given our original mix, except for Ca. One should perhaps not exclude the possibility that the 0.3 dex enrichment for α elements that we used (see § 2) would be inappropriate for Ca.

Abundance isochrones are shown at four ages between 11 and 14 Gyr. This allows an evaluation of the effect of the assumed cluster age on the comparison between the calculated and observed abundances. If the cluster is only 11 Gyr, the expected range of abundance variations around turnoff is larger than at 13.5 Gyr. For Na and Fe, it is approximately 0.3 dex larger. On the other hand, older clusters have smaller star-to-star abundance variations around turnoff.

When comparing surface abundances of turnoff stars to those of giants to high accuracy, one should include the effect of settling of metals from the outer half to the inner half of such stars. That settling (see Paper I, Fig. 5) is deeper than the depth affected by dredge-up. The effect amounts to approximately 0.03 dex at the base of the giant branch when dredge-up has affected the outer 34% of the mass; it goes down to 0.01 dex when dredge-up reaches 60% of the mass. This means that even on the giant branch, the surface abundances of metals are smaller by 0.01–0.03 dex than the initial abundances of metals. This is a small effect but comparable to the claimed accuracy in some recent observational papers (Gratton et al. 2001).

5.3. *M71*

The chemical composition of turnoff, red HB stars, and giants of M71 has been studied in a series of papers (Cohen, Behr, & Briley 2001; Ramirez et al. 2001; Ramirez & Cohen 2002). Their turnoff stars have $T_{\rm eff} = 5800$–5900 K and $\log g = 4.05$–4.15, and the 12 Gyr isochrones seem to reproduce the age of M71 best (Cohen et al. 2001). Ramirez et al. (2001) determine for Fe I, [Fe/H] $= -0.71 \pm 0.08$ and for Fe II, [Fe/H] $= -0.84 \pm 0.12$, where they took averages over all stars they considered. They do not detect variations

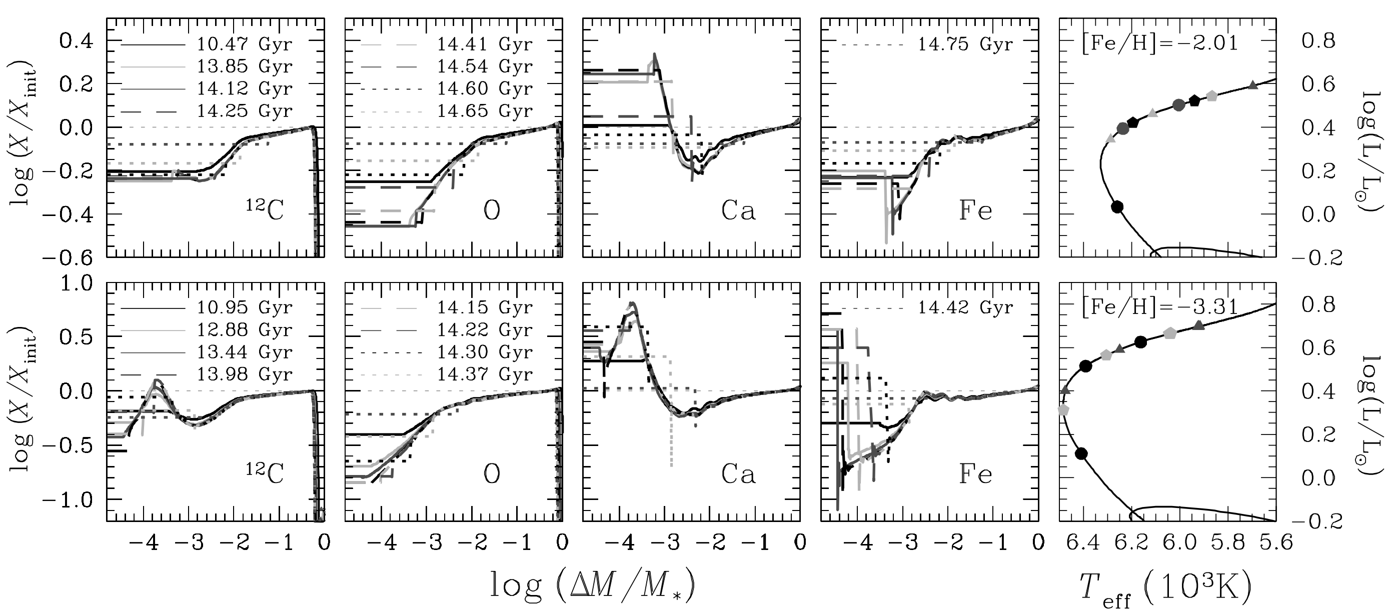

FIG. 13.—Interior profiles of abundance concentrations as a function of $\log \Delta M/M_*$ in 0.77 $M_\odot$ models of [Fe/H] $= -2.01$ (*upper row*) and [Fe/H] $= -3.31$ (*lower row*). The position of each star on the HR around turnoff is indicated in the right-hand part of each row. Curves correspond to different ages and are identified separately in each row. See Fig. 4 of Paper I for a similar figure but for all 28 species in a star with [Fe/H] $= -2.31$. [*See the electronic edition of the Journal for a color version of this figure.*]

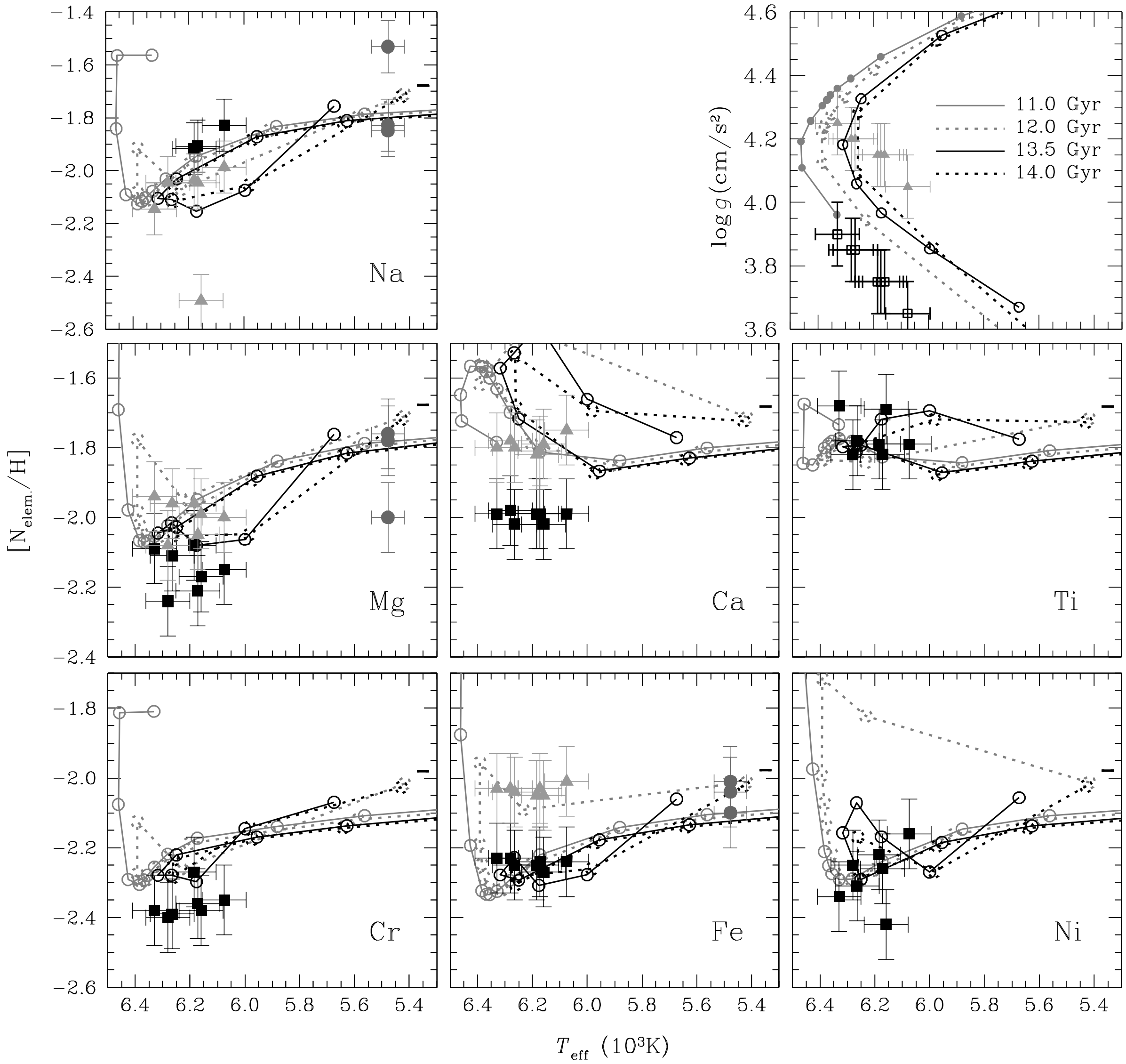

FIG. 14.—In the upper right-hand corner is the T_{eff}- log g diagram obtained at ages from 11 to 14 Gyr with [Fe/H] = −2.01. They are compared to the log g, T_{eff} determined by Thévenin et al. (2001) for their turnoff stars. Both the LTE (*filled squares*) and the NLTE (*filled triangles*) log g are shown. The theoretical isochrones are in between the two sets. In the other parts of the figure, the observationally determined abundances are compared to model predictions. The original abundance is indicated by a small horizontal line close to the right of each part of the figure. When two determinations were done, the gray triangles are the NLTE determinations and the black squares the LTE ones. Since the observed stars are past turnoff, they are generally on the part of the isochrones that ends below 5400 K. So are the subgiants at 5470 K (*filled circles*), which were taken from Gratton et al. (2001). There is an apparent disagreement between observations and the models only for Ca.

in [Fe/H] from one group of stars to the next. Given the error bars, they could not exclude 0.1–0.2 differences between turnoff stars and giants or HB stars. From their Table 4, turnoff stars would have a 0.1 dex smaller [Fe/H] than other groups from Fe I lines but a 0.2 dex larger abundance from Fe II lines. The error bars on the Fe II lines are twice as large as on the Fe I lines. They note no evidence of NLTE effect in agreement with the Thévenin & Idiart (1999) result that these are smaller than 0.1 dex if [Fe/H] > −0.75. The abundance of metals normalized to Fe were observed by Ramirez & Cohen (2002). They studied 22 elements and did not observe any systematic difference in [X/Fe] between the turnoff and the other stars except for expected variations of [Li/H].

These results are in agreement with our discussion of § 4.2 and of Figure 9, in that in 12 Gyr clusters with [Fe/H] = −0.71, [Fe/H] shows only a 0.1–0.15 dex reduction from its value at T_{eff} = 5300 K to that in turnoff stars at T_{eff} = 5900 K. Atomic diffusion is not expected to cause variations in the relative abundances of metals in clusters with [Fe/H] = −0.71.

6. LITHIUM IN FIELD STARS

A simulation of the Li abundance in low-metallicity stars of different ages and metallicities is compared to observations of Li in field halo stars in order to test whether models with atomic diffusion and no turbulence are excluded by the Li observations. We chose to follow an approach similar to that of Salaris & Weiss (2001), who argued that it was premature to conclude that observations of Li alone could exclude the atomic diffusion only model.

We first generated cubes of values for each variable of interest using 98 evolutionary tracks of different mass and metallicity (see Table 1). Metallicity (Z), stellar mass, and a normalized age[3] s are used as axes of each cube. Using cubic splines, points were generated along each track at fixed Δs intervals; the density of points was chosen high enough to ensure that negligible additional inaccuracy follow from quadratic interpolation between them when the interpolation cubes are used later. Similarly, cubic splines were then used to interpolate between different M-values at common s points. Six planes are thus filled with values for all variables of interest, one plane at each Z for which evolutionary tracks were calculated. Tests were made to verify that splines did not introduce spurious variations of one quantity close to rapid variations of that quantity. Values for a given quantity were then obtained by quadratic interpolation in the cube of that quantity.

Stars were generated at random with constraints on their age, metallicity, and mass. We used Becker & Mathews (1983) for the initial mass function of halo stars ($\propto m^{-2.3}$). The spread in age was assumed Gaussian. The distribution of metallicity, Z, was taken from Figure 1 of Laird et al. (1988),[4] but both maximum and minimum metallicity cutoffs were imposed, so that the sample have approximately the same metallicity as observations. Using these three probability distributions, points were generated at random within the three-dimensional cube. In those Monte Carlo simulations the stellar luminosity was further used to take into account the larger volume scanned by surveys as luminosity increases. The function $L^{1.5}$, normalized to 1.0 for the most luminous objects of the sample, was used to define the probability of keeping each of the originally drawn points.

In Figure 15 are shown the results of the simulation for 300 stars in the $\log Z$ interval from -5.0 to -3.1. Each star is plotted with a symbol whose size is a decreasing function of its $\log g$ so as to allow distinguishing subgiants from dwarfs. The L-$T_{\rm eff}$ has a thickness caused by both the age and metallicity ranges chosen. In this simulation, the age distribution of field halo stars was assumed to be a Gaussian centered around 13.5 Gyr, the age determined in Paper II for M92. The standard deviation was assumed to be 0.5 Gyr. On the subgiant branch, the lowest allowed $\log g$ is 3.9, in order to limit the sample to the type of stars included in Spite, Maillard, & Spite (1984) and Ryan et al. (1999).

On the lower part of Figure 15 is shown the $T_{\rm eff}$ dependence of A(Li) for the sample. One can distinguish the main-sequence and subgiant stars by the size of the symbol. The main-sequence lithium abundance for $T_{\rm eff} \leq 5800$ K shows a visible thickness of about 0.05 dex at a given $T_{\rm eff}$ coming from both the Z and age ranges. Above 5800 K, the largest value of A(Li) at each $T_{\rm eff}$ progressively decreases, and the thickness of the A(Li) distribution progressively increases. One is close to the turnoff, which does not occur at exactly the same $T_{\rm eff}$ for all metallicities, leading to an increase in the interval of $T_{\rm eff}$ where a large range of A(Li) is expected. Since there is a well-defined upper envelope in A(Li) versus $T_{\rm eff}$, taking a smaller sample of stars could never lead to a smaller reduction than the upper limit. The presence of the Spite plateau (Spite et al. 1984), which was confirmed by Ryan et al. (1999), is consequently a strong argument for the presence of some hydrodynamic process competing with atomic diffusion below the surface convection zone of Population II stars as discussed in Paper I. One could also increase the initial Li abundance 0.2 dex, thus forcing agreement with the observations of Ryan et al. (1999) by shifting all calculated points upward 0.2 dex. However, between 5600 and 6000 K, the calculated points would then agree only with the two larger A(Li) values and would so disagree with most observations of Spite et al. (1984). While in our sample some of the subgiants (the larger circles in Fig. 15), between 5800 and 6000 K can have lower A(Li) than the dwarfs (the smaller circles), one expects very few of those subgiants in our Monte Carlo simulation. It does not appear likely to us that uncertainties in the $T_{\rm eff}$ scale would have conspired with sample size to make A(Li) appear constant as a function of $T_{\rm eff}$. As suggested by Salaris & Weiss (2001), it may require, however, a larger sample size to transform this strong argument into a proof.

In Table 1 of Ryan et al. (2001a) are listed the $T_{\rm eff}$, A(Li), and [Fe/H] of many Li-poor stars. Most could be explained by atomic diffusion if the age of some of them is smaller than 13.5 Gyr. They would correspond to those stars that have just passed turnoff and that appear below $A(\mathrm{Li}) = 1.5$. This would require that the mixing that keeps A(Li) constant before turnoff become less efficient past turnoff.

In the upper right part of the figure are shown the A(Be) as a function of A(Li). Note the slope of about 0.7 for the dwarfs stars, but as turnoff is approached, Be becomes supported by $g_{\rm rad}$(Be) and its abundance rises. It is a sensitive function of $T_{\rm eff}$, while A(Li) is constant at around 1.4.

7. CONCLUSION

It has been shown that not only are $g_{\rm rad}$ important in the highest $T_{\rm eff}$ stars of globular clusters of low metallicity, but that this importance varies strongly with metallicity. The effect of atomic diffusion on the concentrations of chemical species in turnoff stars is then a sensitive function of the cluster's metallicity. Metals and even LiBeB are supported by $g_{\rm rad}$ in low-metallicity high $T_{\rm eff}$ stars in which Deliyannis, Demarque, & Kawaler (1990), Chaboyer et al. (2001), and Salaris & Weiss (2001) conclude there should be the largest *underabundances*.

As a general rule, diffusion should lead to 0.1–0.2 dex reduction in metal abundances in dwarfs and subgiants of $T_{\rm eff} \leq 6000$ K, while above that $T_{\rm eff}$, there can be considerable star-to-star variation because of diffusion (see § 4.2). Overabundances compared to original abundances become large for many metals when the original $[\mathrm{Fe/H}] \leq -2.31$. As discussed in Paper I, such anomalies might already have

[3] The normalized age is a logarithmic time variable defined by $s = (t - t_0)/(t_1 - t_0)$, where $t = \log_{10}$ (real age, in years) and $t_0 = -2.4317M + 0.6490M^3 + 73.2105Z + 0.0006Z^3 + 8.9295$, $t_1 = -2.4552M + 0.0920M^3 + 36.3665Z + 0.0003Z^3 + 11.9627$, where M is the stellar mass in solar units, and Z is the desired zero-age metals mass fraction. This age transformation was determined by least-squares fit to bring the beginning and the end of the main sequence for all tracks to the same standard values of $s = 0$ and $s = 1$, respectively. This variable was introduced for the sole purpose of improving interpolations between evolutionary tracks of different M and Z, which have strongly varying age coverage. For a given s, interpolating in M and Z interpolates between models with roughly similar structures. We let s go slightly beyond 1.0, up to 1.1, which corresponds approximately to the base of the giant branch. Since t and s are linearly related for given M and Z, this relation can be inverted trivially to give the real stellar age corresponding to any point within the interpolation cube.

[4] Their metallicity variable represents *observed* $[m/\mathrm{H}]$; we used the same distribution to generate *initial* (zero-age) metallicities, with $\log Z_0 =$ their $\log z - 1.7$.

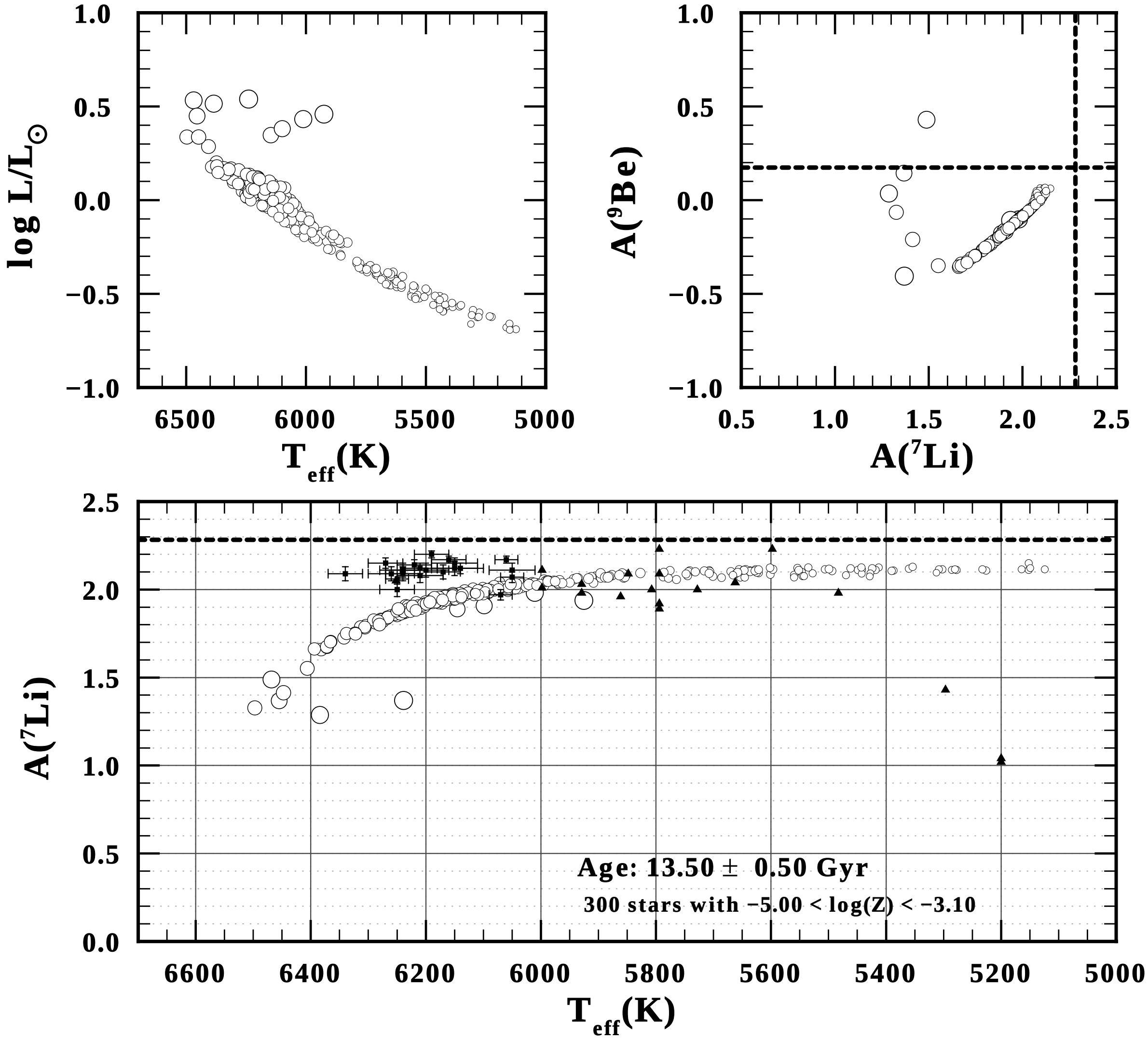

FIG. 15.—Simulation of 13.5 Gyr halo field stars and, in the lower part, comparison to the observations of Ryan et al. (1999, *squares*) and Spite et al. (1984, *triangles*). Open circles represent simulated stars, while filled circles represent observations. The horizontal dashed line gives the initial Li abundance used in the calculations. No pre–main-sequence destruction of Li is included in these calculations. It could lead to a reduction of A(Li), especially below 5500 K.

been observed in M92. They could be important in low-metallicity halo field stars. In more metal-rich clusters, however, few, if any, overabundances should be expected. For instance, for Fe, the presence of $g_{\rm rad}$ considerably reduces settling without causing overabundances around turnoff in clusters whose original [Fe/H] ≥ -2.01. Underabundances by up to -0.3 dex are still expected in the absence of turbulence but that is only 0.1–0.2 dex larger than in the lower $T_{\rm eff}$ subgiants. It may partially explain the absence of observation of variations of the abundances of [Fe/H] in NGC 6397 and M71 (Ramirez et al. 2001 and Gratton et al. 2001). Even in clusters whose original [Fe/H] ≥ -2.01, [X/Fe] is expected to vary significantly in stars with $T_{\rm eff} \geq 6000$ K for some species. Such variations (see § 5) are in reasonable agreement with the observations of Gratton et al. (2001) (for instance for [Mg/Fe]) but disagree with the [Ca/Fe] observation of Thévenin et al. (2001). For most metals the situation remains ambiguous: observations, taking into account the error bars, do not yet require additional hydrodynamic processes to compete with atomic diffusion. Even in giants a generalized reduction of metals by 0.01–0.03 dex is expected (see § 5.2). We do not compare our results with abundance observed in clusters such as NGC 6752, where abundance variations observed in giants complicate the comparison.

Among low-metallicity halo field stars, the surface chemical composition of the star CD $-24°17504$, which has [Fe/H] $= -3.37$, $T_{\rm eff} = 6070$ K, and $\log g = 3.6$ according to Norris et al. (2001), could have been substantially modified by diffusion and $g_{\rm rad}$ (see Figs. 10 and 11 of this paper). The four other stars they observed have sufficiently low $T_{\rm eff}$ and $\log g$ not to have had the relative values of surface abundances of different metals significantly modified by diffusion processes. Since, among those four stars, there are considerable star-to-star variations of the relative abundances, it is difficult to do any meaningful comparison of observations of halo field stars with diffusion calculations. However, since diffusion could have modified the relative metal abundances of CD $-24°17504$, this star should be used with more caution than the others in comparing to the products of nucleosynthesis. The comparisons in Figures 5–8 of Norris et al. (2001) could be affected insofar as stars close enough to turnoff are involved.

7.1. *Turbulence*

All calculations presented in this paper were done from first principles. Nowhere have the effects of turbulence been included in the calculations. It is useful, however, to briefly discuss in this section the potential effects of turbulence on our results. We use the parametrization and results of Paper I, where these effects had been studied for a cluster with $[Fe/H] = -2.31$.

As seen in Figure 6 of Paper I, the parametrized turbulence chosen to minimize Li abundance variation in the atmosphere mixes the star from the surface down to a layer where $\log T \simeq 6.3$. Assuming the same parametrization, one may use the values of $\log T_{\rm bcz}$ in Figure 1 to predict the expected effect of that turbulence model on the anomalies caused by diffusion. Since in models with $[Fe/H] = -0.71$, $\log T_{\rm bcz} \geq 6.2$ throughout the evolution of all models with $M \leq 0.9\ M_{\odot}$, the parametrization of turbulence used in Paper I would not have significantly modified the evolution of concentrations in stars of that metallicity. This is confirmed by comparing the abundance isochrones in Figures 13 and 14 of Paper I for the turbulence model labeled T6.09 with those of Figures 9, 10, and 11 of this paper for the metallicity of $[Fe/H] = -0.71$. Over the $T_{\rm eff}$ interval where both groups have stars ($T_{\rm eff} \leq 5900$ K), the anomalies are very similar. In the lower metallicity case (Paper I, Figs. 13 and 14), there are stars at $T_{\rm eff} > 6000$ K that are not present at higher metallicity. In these, with the turbulence model labeled T6.09, the underabundances vary between -0.1 and -0.2 dex. The reduction of some of the underabundances is caused by the nonnegligible albeit small role of $g_{\rm rad}$.

For other metallicities, the use of a similar parametrization would have led to a similar variation of surface concentrations of metals. In all cases, one would have a 0.10–0.15 dex settling of metals in main-sequence Population II stars with $T_{\rm eff} < 5900$ K, as seen above for stars with metallicity $[Fe/H] = -0.71$ and 0.1–0.2 dex at higher $T_{\rm eff}$. This reduction of metallicity would disappear when stars go up the giant branch. They become equal to about 0.1 dex at $T_{\rm eff} = 5600$ K and smaller than 0.03 dex for $T_{\rm eff} = 5400$ K. We did not repeat, for different metallicities, the calculations with turbulence, as described in Paper I, since the result would be nearly the same. The constancy of the Li abundance in metal-poor Population II stars with $T_{\rm eff} > 5500$ K is a strong argument for the presence of such a mixing in most of those stars (although its presence is not proven; see § 6). *There then remains an effect of settling of at least 0.1 dex for all metals. According to Paper I the reduction is of about 0.2 dex for* Li. According to Figure 15, the reduction of $A(\rm Li)$ at 5600 K in absence of turbulence is 0.16–0.20 dex depending on metallicity. Using one optimal parametrization of turbulence for all masses of a given metallicity led in Paper I to some Li destruction in stars with $T_{\rm eff} \leq 5600$ K (note the differences between the three curves in Fig. 15 of Paper I), so that $A(\rm Li)$ is at least 0.20 dex smaller than the initial value.

Overabundances of metals would then be expected only in those hot turnoff stars that would be the equivalent of the Population I AmFm stars. They would have smaller turbulence than most turnoff stars. They might already have been observed in M92.

We thank A. Weiss for his constructive comments that lead to significant improvements of this paper. This research was partially supported at the Université de Montréal by NSERC. We thank the Réseau Québécois de Calcul de Haute Performance (RQCHP) for providing us with the computational resources required for this work.

REFERENCES

Bahcall, J. N., Pinsonneault, M. H., & Wasserburg, G. J. 1995, Rev. Mod. Phys., 67, 781
Becker, S. A., & Mathews, G. J. 1983, ApJ, 270, 155
Boesgaard, A. M., Deliyannis, C. P., Stephens, A., & King, J. R. 1998, ApJ, 493, 206
Brun, A. S., Turck-Chièze, S., & Zahn, J. P. 1999, ApJ, 525, 1032
Carretta, E., & Gratton, R. G. 1997, A&AS, 121, 95
Carretta, E., Gratton, R., Cohen, J. G., Beers, T. C., & Christlieb, N. 2002, AJ, 124, 481
Castilho, B. V., Pasquini, L., Allen, D. M., Barbuy, B., & Molaro, P. 2000, A&A, 361, 92
Chaboyer, B., Fenton, W. H., Nelan, J. E., Patnaude, D. J., & Simon, F. E. 2001, ApJ, 562, 521
Charbonnel, C., Vauclair, S., & Zahn, J.-P. 1992, A&A, 255, 191
Christensen-Dalsgaard, J., Proffitt, C. R., & Thompson, M. J. 1993, ApJ, 403, 75
Cohen, J. G., Behr, B. B., & Briley, M. M. 2001, AJ, 122, 1420
Deliyannis, C. P., Demarque, P., & Kawaler, S. D. 1990, ApJS, 73, 21
Freytag, B., & Salaris, M. 1999, ApJ, 513, L49
Gonzalez, J.-F., LeBlanc, F., Artru, M.-C., & Michaud, G. 1995, A&A, 297, 223
Gratton, R. G., et al. 2001, A&A, 369, 87
Guenther, D. B., Kim, Y.-C., & Demarque, P. 1996, ApJ, 463, 382
Guzik, J. A., & Cox, A. N. 1992, ApJ, 386, 729
———. 1993, ApJ, 411, 394
Jehin, E., Magain, P., Neuforge, C., Noels, A., Parmentier, G., & Thoul, A. A. 1999, A&A, 341, 241
King, J. R., Stephens, A., Boesgaard, A. M., & Deliyannis, C. F. 1998, AJ, 115, 666
Laird, J. B., Carney, B. W., Rupen, M. P., & Latham, D. W. 1988, AJ, 96, 1908
LeBlanc, F., Michaud, G., & Richer, J. 2000, ApJ, 538, 876
Michaud, G. 1970, ApJ, 160, 641
Michaud, G., Fontaine, G., & Beaudet, G. 1984, ApJ, 282, 206
Michaud, G., & Proffitt, C. R. 1993, in IAU Colloq. 137, Inside the Stars, ed. W. W. Weiss & A. Baglin (ASP Conf. Ser. 40; San Francisco: ASP), 246
Minniti, D., Geisler, D., Peterson, R. C., & Claria, J. J. 1993, ApJ, 413, 548
Norris, J. E., Beers, T. C., & Ryan, S. G. 2000, ApJ, 540, 456
Norris, J. E., Ryan, S. G., & Beers, T. C. 2001, ApJ, 561, 1034
Paquette, C., Pelletier, C., Fontaine, G., & Michaud, G. 1986, ApJS, 61, 177
Pinsonneault, M. H., Deliyannis, C. P., & Demarque, P. 1992, ApJS, 78, 179
Pinsonneault, M. H., Walker, T. P., Steigman, G., & Narayanan, V. K. 1999, ApJ, 527, 180
Proffitt, C. R. 1994, ApJ, 425, 849
Proffitt, C. R., & Michaud, G. 1991, ApJ, 371, 584
Qian, Y.-Z., Sargent, W. L. W., & Wasserburg, G. J. 2002, ApJ, 569, L61
Ramirez, S. V., & Cohen, J. G. 2002, AJ, 123, 3277
Ramirez, S. V., Cohen, J. G., Buss, J., & Briley, M. M. 2001, AJ, 122, 1429
Richard, O., Michaud, G., & Richer, J. 2001, ApJ, 558, 377
Richard, O., Michaud, G., Richer, J., Turcotte, S., Turck-Chièze, S., & VandenBerg, D. A. 2002, ApJ, 568, 979 (Paper I)
Richard, O., Vauclair, S., Charbonnel, C., & Dziembowski, W. A. 1996, A&A, 312, 1000
Richer, J., Michaud, G., Rogers, F., Iglesias, C., Turcotte, S., & LeBlanc, F. 1998, ApJ, 492, 833
Ryan, S. G., Beers, T. C., Kajino, T., & Rosolankova, K. 2001a, ApJ, 547, 231
Ryan, S. G., Kajino, T., Beers, T. C., Suzuki, T. K., Romano, D., Matteucci, F., & Rosolankova, K. 2001b, ApJ, 549, 55
Ryan, S. G., Norris, J. E., & Beers, T. C. 1999, ApJ, 523, 654
Salaris, M., & Weiss, A. 2001, A&A, 376, 955
Spite, F., & Spite, M. 1982, A&A, 115, 357
Spite, M., Maillard, J.-P., & Spite, F. 1984, A&A, 141, 56

Théado, S., & Vauclair, S. 2001, A&A, 375, 70
Thévenin, F., Charbonnel, C., de Freitas Pacheco, J. A., Idiart, T. P., Jasniewicz, G., de Laverny, P., & Plez, B. 2001, A&A, 373, 905
Thévenin, F., & Idiart, T. P. 1999, ApJ, 521, 753
Thoul, A., Jorissen, A., Goriely, S., Jehin, E., Magain, P., Noels, A., & Parmentier, G. 2002, A&A, 383, 491
Turcotte, S., Richer, J., & Michaud, G. 1998a, ApJ, 504, 559
Turcotte, S., Richer, J., Michaud, G., Iglesias, C., & Rogers, F. 1998b, ApJ, 504, 539
VandenBerg, D. A., Richard, O., Michaud, G., & Richer, J. 2002, ApJ, 571, 487 (Paper II)
VandenBerg, D. A., Swenson, F. J., Rogers, F. J., Iglesias, C. A., & Alexander, D. R. 2000, ApJ, 532, 430
Vauclair, S., & Charbonnel, C. 1995, A&A, 295, 715
Zinn, R., & West, M. J. 1984, ApJS, 55, 45